Uncovering neuromesodermal progenitor contributions to neural crest derivatives *in vivo*

A Thesis

submitted to

Indian Institute of Science Education and Research Pune

in partial fulfilment of the requirements for the BS-MS Dual Degree Programme

by

Manas M. Raikar

20201042

Indian Institute of Science Education and Research Pune

Dr. Homi Bhabha Road,

Pashan, Pune 411008, INDIA.

Date: 16 March, 2025

Under the guidance of

Supervisor: **Prof. Tatjana Sauka-Spengler**,

Investigator, Stowers Institute for Medical Research, Kansas City, MO, USA

From May 2024 to Mar 2025

INDIAN INSTITUTE OF SCIENCE EDUCATION AND RESEARCH PUNE

Certificate

This is to certify that this dissertation entitled "**Uncovering neuromesodermal progenitor contributions to neural crest derivatives *in vivo***" towards the partial fulfilment of the BS-MS dual degree programme at the Indian Institute of Science Education and Research, Pune represents study/work carried out by **Manas Raikar** at the Stowers Institute for Medical Research under the supervision of **Prof. Tatjana Sauka-Spengler**, Investigator, Stowers Institute for Medical Research, during the academic year 2024-2025.

Prof. Tatjana Sauka-Spengler

Committee:

Prof. Tatjana Sauka-Spengler

Dr. Krishanpal Karmodiya

This thesis is dedicated to the institution of Science

Declaration

I hereby declare that the matter embodied in the report entitled "**Uncovering neuromesodermal progenitor contributions to neural crest derivatives *in vivo***" are the results of the work carried out by me at the Stowers Institute for Medical Research, Kansas City, USA under the supervision of Prof. Tatjana Sauka-Spengler, and the same has not been submitted elsewhere for any other degree. Wherever others contribute, every effort is made to indicate this clearly, with due reference to the literature and acknowledgement of collaborative research and discussions.

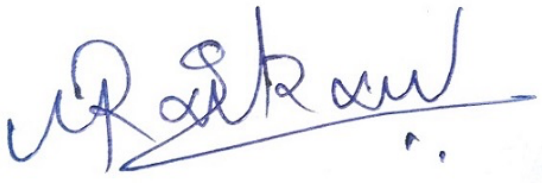

Name of Student – Manas M. Raikar

Roll # – 20201042

Institution – IISER Pune

Table of Contents

List of Figures

1. Abstract

The neural crest (NC) is a multipotent embryonic cell population contributing to craniofacial skeleton, peripheral nervous system (PNS), and body pigmentation in vertebrate embryos. NC cells delaminate from the dorsal neural tube, and their fate is dictated by their anterior-posterior axis location. Neuromesodermal progenitors (NMPs) are a distinct posterior embryonic cell population giving rise to paraxial mesoderm and central nervous system (CNS) lineages. In vitro studies using pluripotent stem cells show that trunk-like NC derivatives require an intermediate state expressing both NC and NMP markers. The in vivo link between trunk NC and NMPs remains elusive, raising questions about the role of NMPs in specifying trunk peripheral neuronal populations, traditionally thought to derive from NC.

We employed a Cre-Lox based genetic lineage tracing approach to track NMP derivatives in the zebrafish embryo and larva at a high resolution through constitutive labelling. We performed single-cell and single-nuclear RNA-sequencing to generate a comprehensive time-resolved single-cell atlas of NMP derivatives in the zebrafish larva.

We identify an unprecedented range of NMP derivatives. NMPs differentiate into CNS neurons and glia, skeletal and muscle elements, myeloid, vasculature and many others. Notably, we discover contributions to the PNS, including sympathetic, enteric, and autonomic neurons and a Schwann cell precursor population, previously thought to be entirely NC-derived. We identify and characterize specific neuronal populations based on their marker gene expression through integrative analysis with publicly available scRNA-seq datasets.

Therefore, in this study, we uncover the broad developmental potential of NMPs and establish NMPs as a paradigm for studying complex cell fate decisions, which would have implications on advancing regenerative cell therapies.

2. Acknowledgments

Firstly, I am immensely grateful to my supervisor, Prof. Tatjana Sauka-Spengler for the opportunity to pursue this project, her invaluable mentorship, knowledgeable critique and her will to help me realise my full potential as a researcher. She has deeply influenced me and made into a better scientist than I was a year ago. I would also like to thank my mentor, Dr. Seda Ateş-Kalkan for teaching me the techniques for the project, collaborating with me, and for her support and understanding. I will miss all the fun chats we had while doing experiments on the bench! Huge thanks to all the TSS lab members; Kurne, Joseph, Erin, Chloe, Yuri, An, Zixuan, Evgeny, Carrie, Julianna, Serenity, and Hanifi and the Oxford lab for the thoughtful comments, suggestions and the fun camaraderie, with a shoutout to Justin for his enteric nervous system expertise.

I would like to thank my expert member Dr. Krishanpal Karmodiya, not just for his feedback and questions on my work and presentation, but also for being an amazing supervisor and mentor during my time at IISER. I would also like to acknowledge the core facilities at Stowers Institute for Medical Research; Computational Biology, Cytometry, Sequencing and Discovery Genomics and the Zebrafish team for all the great facilities. Special thanks to Andrew from Computational Biology for helping me get started with single-cell analysis as someone who had never had written code for any project. I would like to acknowledge the funding agencies, KVPY for funding my IISER education and the Stowers Institute for funding the work presented in this thesis.

I would also like to thank all my friends in Kansas City; Amruta, Kurne, Atharva, Shrutika, and Krish, for helping maintain my sanity and for being a family away from home. Special thanks to Amruta for always listening to me ramble about some cool talk I heard and her critical feedback on my work and on my thesis. Heartfelt gratitude to all my IISER friends (batchmates, seniors, juniors and Krish lab members) too many to name, for the thought-provoking late-night discussions and fantastic memories during my time in the IISER campus. Last but not the least, thanks to my parents for their unconditional love and support throughout this year and throughout life.

3. Contributions

Contributor name	Contributor role
TSS	Conceptualization Ideas
TSS, SAK	Methodology
MMR	Software
MMR, SAK	Validation
MMR	Formal analysis
MMR, SAK	Investigation
MMR, SAK, TSS	Resources
MMR	Data Curation
MMR	Writing - original draft preparation
MMR, TSS	Writing - review and editing
MMR, SAK	Visualization
SAK, TSS	Supervision
TSS	Project administration
TSS	Funding acquisition

Chapter 1 Introduction

1.1 The Neural Crest (NC)

The Neural Crest (NC) is a characteristic population of multipotent cells with a diverse developmental potential. Unique to the vertebrate lineage, the NC is specified along the entire antero-posterior (AP) axis in the developing early neural plate border (NPB), located at the interface between the neural and non-neural parts of the ectoderm. As the neural plate forms the neural tube, through a process called neurulation, these NC cells delaminate via an epithelial-to-mesenchymal transition (EMT) from the dorsal aspect of the neural tube and migrate to different parts of the embryonic body. After reaching their precise locations, these form various cell types including craniofacial skeletal tissue, cardiomyocytes, peripheral and enteric neurons and glia, melanocytes, and secretory cells of the adrenal medulla (Douarin and Kalcheim, 1999; Simões-Costa and Bronner, 2015). Due to their relatively late origin and due to the vast number of cell types they generate, the NC is also sometimes referred to as the 4th germ layer (Hall, 2000).

The NC is a heterogeneous population based on spatial location along the AP axis. Broadly, the NC can be distinguished into cranial, vagal, trunk and sacral NC subpopulations. The terminal fate of the NC derivatives is influenced by their position along the AP axis. These different subpopulations give rise to a large variety of distinct derivative cell types, for example, the cranial NC forms large parts of the craniofacial skeleton, including chondrocytes, osteocytes and other ectomesenchymal cell types in addition to contributing to cranial ganglia. The vagal NC is responsible for the formation of almost the entire enteric nervous system (ENS) and has contributions to cardiomyocytes of the heart, vasculature, parafollicular cells, etc. The trunk NC primarily gives rise to neural cell types like the dorsal root ganglia, sympathetic chain ganglia, chromaffin cells of the adrenal medulla, and glial cells. The sacral NC, which is believed to be present in amniotes also contributes to the posterior parts of the ENS. All the subpopulations also distinctly give rise to pigment cells (Sauka-Spengler and Bronner-Fraser, 2008; Betancur *et al.*, 2010). Due to its broad developmental potential, the NC has been of interest in stem cell studies as a prospective avenue for developing stem cell therapeutics (Achilleos and Trainor, 2012; Olmsted and Paluh, 2021).

1.2 Neural Crest-derived neuronal cell types

The NC gives rise to a broad range of neuronal derivatives throughout the body of the organism. While the cranial NC produces ectomesenchymal cell types in addition to neurons (Schilling and Kimmel, 1994; Wada *et al.*, 2005; Kague *et al.*, 2012), the posterior NC subpopulations, specifically the trunk NC is solely devoted to producing neuronal and neurosecretory cell types (Lee *et al.*, 2013a; Lee *et al.*, 2013b), the basis of this heterogeneity remaining unknown. Among the posterior NC populations, the vagal NC gives rise to the ENS and the trunk NC gives rise to the sympathoadrenal system, which are at the focus of this study.

The ENS is the largest subdivision of the peripheral nervous system (PNS) and is often referred to as the second brain (Gershon, 1999). In amniotes, the ENS is composed of two different plexuses, the submucosal and the myentric plexus, each forming a complex network of diverse neuronal subtypes (Nagy and Goldstein, 2017). In zebrafish, however, the ENS is only comprised of the myentric plexus, providing a simplistic system to study the principles underlying ENS development. During embryonic development, the ENS is derived from the vagal NC which begins migration from the caudal hindbrain region and invades the foregut of developing 31 hours post-fertilization (hpf) embryos and forms a fully functioning mature ENS by 5 days post-fertilization (dpf) (Shepherd and Eisen, 2011; Ganz, 2018). Some studies have also suggested the contribution of NC-derived Schwann Cell Precursors (SCPs) as a putative progenitor population that contributes to the ENS (El-Nachef and Bronner, 2020). Several developmental studies have uncovered the roles of genes, specifically transcription factors (*phox2bb, phox2a, sox10, hand2, ascl1a/b, zeb2a*) and signalling molecules (*ret, gfra1/2, ednrba/b, notch*) that respond to attractive cues like Glial Derived Neurotrophic Factor (GDNF) (Homma *et al.*, 2000; Barlow *et al.*, 2003)) that play a crucial role in ENS development (Obermayr *et al.*, 2013).

Another crucial neuronal population derived from trunk NC is the sympathetic chain ganglia and the chromaffin cells of the adrenal medulla, which arise from a common progenitor cell population called the sympathoadrenal NC cells. These cells are derived from the trunk NC and migrate ventrally, condensing at specific sites around the dorsal aorta to form the sympathetic chain ganglia in the developing embryo. Another subpopulation migrates further around the aorta to form the adrenal medulla. Although the sympathoadrenal cells start migrating during early larval development in zebrafish, the completely functional sympathetic nervous system is only formed at about 4 weeks of age. While migrating, these cells are receptive to Neuregulin-1 (*nrg1*),

through ErbB2 and ErbB3 receptor signalling. This activates a cascade of transcription factors which, similar to the ENS, involves *phox2a/b, ascl1a/b, hand2, sox10* and additionally includes *insm1* and *gata2/3* (Stewart et al., 2004; Morrison et al., 2016). Furthermore, similar to the ENS, the sympathoadrenal system is also contributed to by SCPs (Furlan and Adameyko, 2018; Kastriti *et al.*, 2022), which also contribute to parasympathetic neurons and other neuronal cell types.

1.3 The Neural Crest Gene Regulatory Network (NC-GRN)

Due to its extraordinary heterogeneity and plasticity, decades of research have tried to uncover critical factors in the gene regulatory network (GRN) underlying NC development. The core GRN is largely conserved among vertebrates and is broadly divided into three modules: a signalling module which includes factors (BMPs, FGFs and Wnt ligands) involved in signalling and induction of the early NPB; an NPB module which involves the transcription factors (*pax3, tfap2a, zic3, msxBCE*) for determining the NPB separately from other ectodermal populations; and finally a NC specification module (*foxd3, snai1b, sox10, sox9a/b*) involving bonafide NC marker genes which further determine the NC within the NPB and play a role in regulating their EMT and migration. *foxd3* is one of the bonafide NC specifiers which plays a crucial role in NC development (Simões-Costa and Bronner, 2015; Rocha *et al.*, 2020).

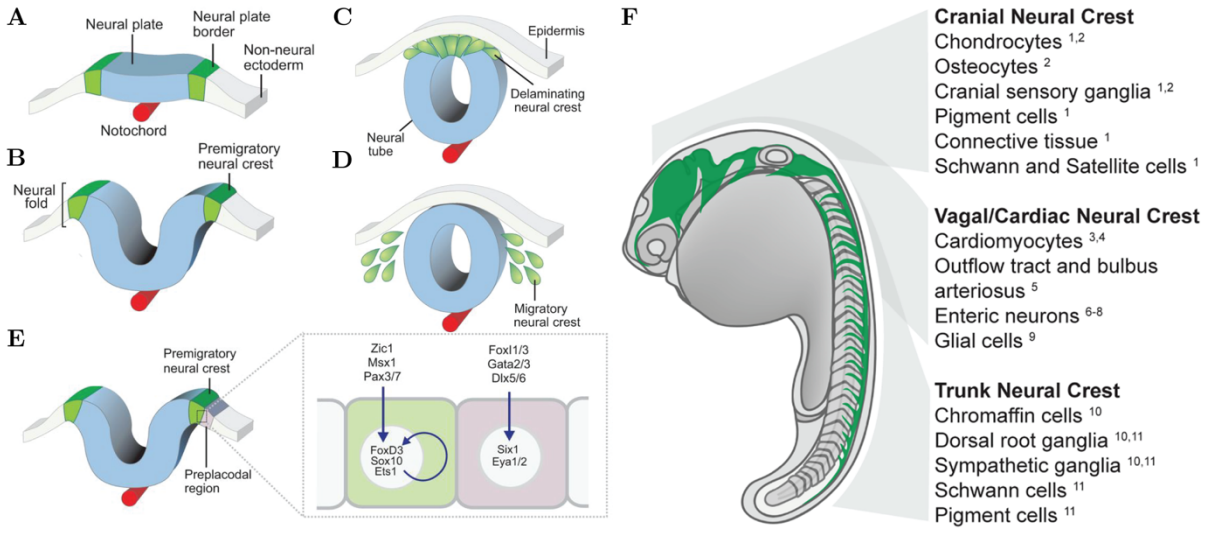

Figure 1 – NC development in vertebrates - (A-D) The developmental specification, EMT, and migration of the NC proceeding simultaneously with neurulation. (E) Gene regulatory network components required for NC

specification, of which *foxd3* plays a crucial role. Panels A-E are adapted from (Simões-Costa and Bronner, 2015). (F) The diverse derivative cell types derived from different NC subpopulations. The sacral NC is considered to be absent in zebrafish. Panel F adapted from (Rocha *et al.*, 2020).

1.4 Role of FoxD3 in NC specification

The winged-helix, forkhead transcription factor *FoxD3* is an important stem cell factor, which performs various functions in different contexts during vertebrate development. Several *in vitro* studies have highlighted the role of *FoxD3* in transcriptional repression in embryonic stem (ES) cells which helps in maintaining their pluripotent cell state (Krishnakumar *et al.*, 2016; Respuela *et al.*, 2016). *In vivo*, *FoxD3* being a stem cell factor, is one of the earliest genes showing zygotic expression in the zebrafish embryo. *FoxD3* expression has been observed in multiple phases, the first one being expressed during epiboly in the ectoderm and dosrsal mesendoderm, followed by the NPB, tailbud mesoderm, and floor plate. The second phase involves *FoxD3* expression throughout the AP axis in premigratory NC cells which gets restricted to a subset of migrating cranial NC but not trunk NC cells. Despite the downregulation of *FoxD3* in migratory trunk NC, studies have observed its reappearance in certain trunk NC derived tissues, like peripheral neurons and glia and other tissues like the somites (Odenthal and Nüsslein-Volhard, 1998).

FoxD3 has also been shown to play a bimodal role during NC development in zebrafish. Acting as a pioneer transcription factor in premigratory NC, *FoxD3* is involved in binding chromatin and establishing chromatin accessibility at several NC-specific loci across the genome. This pioneering activity is followed by its previously characterised role as a transcriptional repressor, which aids in maintaining pluripotency and preventing premature migration and differentiation into neuronal NC derivatives (Lukoseviciute *et al.*, 2018).

A subsequent study found differential regulation of *FoxD3* in the context of NC development in zebrafish. The authors found that two different autoregulatory enhancers are responsible for driving the anterior and posterior domains of *FoxD3* expression in the zebrafish embryo. However, they found that although the anterior enhancer marked cranial NC, the posterior enhancer marked bipotent neuromesodermal progenitors (NMPs). They found evidence of NMPs forming bonafide trunk neural crest derivatives and proposed an alternative non-NPB origin of the posterior trunk NC in zebrafish (Lukoseviciute *et al.*, 2021). This model proposes a novel mechanism for the dichotomy in the origin of and consequently in the cell types

formed by the cranial and trunk NC, which is distinct from the mechanism proposed in the chick embryo (Simões-Costa *et al.*, 2012).

1.5 Neuromesodermal Progenitors (NMPs)

Neuromesodermal Progenitors (NMPs) are a population of bipotent axial progenitors which are located in the early tailbud region of the early embryo. These cells, identified as a *Sox2+* and *Brachyury+* population, contribute to the pre-neural tube and are capable of acquiring spinal cord neuron and paraxial mesoderm cell fates (Tzouanacou *et al.*, 2009; Sambasivan and Steventon, 2021; Wymeersch *et al.*, 2021).

Previous studies attempting to model NC development using human embryonic stem cells *in vitro*, predominantly observed formation of cranial NC-like cells but not trunk NC-like cells. Successful attempts at *in vitro* differentiation of trunk NC-like cells achieved it only via a transient NMP-like state. Additionally, studies attempting to generate *in vitro* trunk NC models through using Wnt and FGF ligands, which emulate an NPB origin, observe an intermediate cell state expressing both early NC and NMP markers (Frith *et al.*, 2018; Gomez *et al.*, 2019; Hackland *et al.*, 2019). NMP-derived posterior NC populations have also been demonstrated to rescue disease phenotype in a mouse model for Hirschsprung disease (Fan *et al.*, 2023). However, *in vitro* differentiation studies have limitations in replicating heterogenous *in vivo* cell fate decisions. Some *in vivo* studies in avian and mammalian embryos, including classical chimeric lineage tracing and fate mapping experiments, have also hinted towards an alternative origin of posterior NC regions from heterogenous tailbud progenitor populations (Schoenwolf and Nichols, 1984; Catala *et al.*, 1995).

However, the diversity of derivative cell types generated by NMPs during zebrafish embryonic development, and consequently the NC derivatives contributed by NMPs along with their underlying gene regulatory mechanism, remains unknown. An ongoing study in the lab has used a Cre-Lox based genetic lineage tracing approach to track NMP derivatives through zebrafish development by constitutively labelling of NMPs. Using this transgenic line, we performed immunofluorescence staining to search for NMP-derived NC derivatives and found NMP contributions to the enteric and sympathetic nervous system, both canonically thought to derive from the NC (Figure 2).

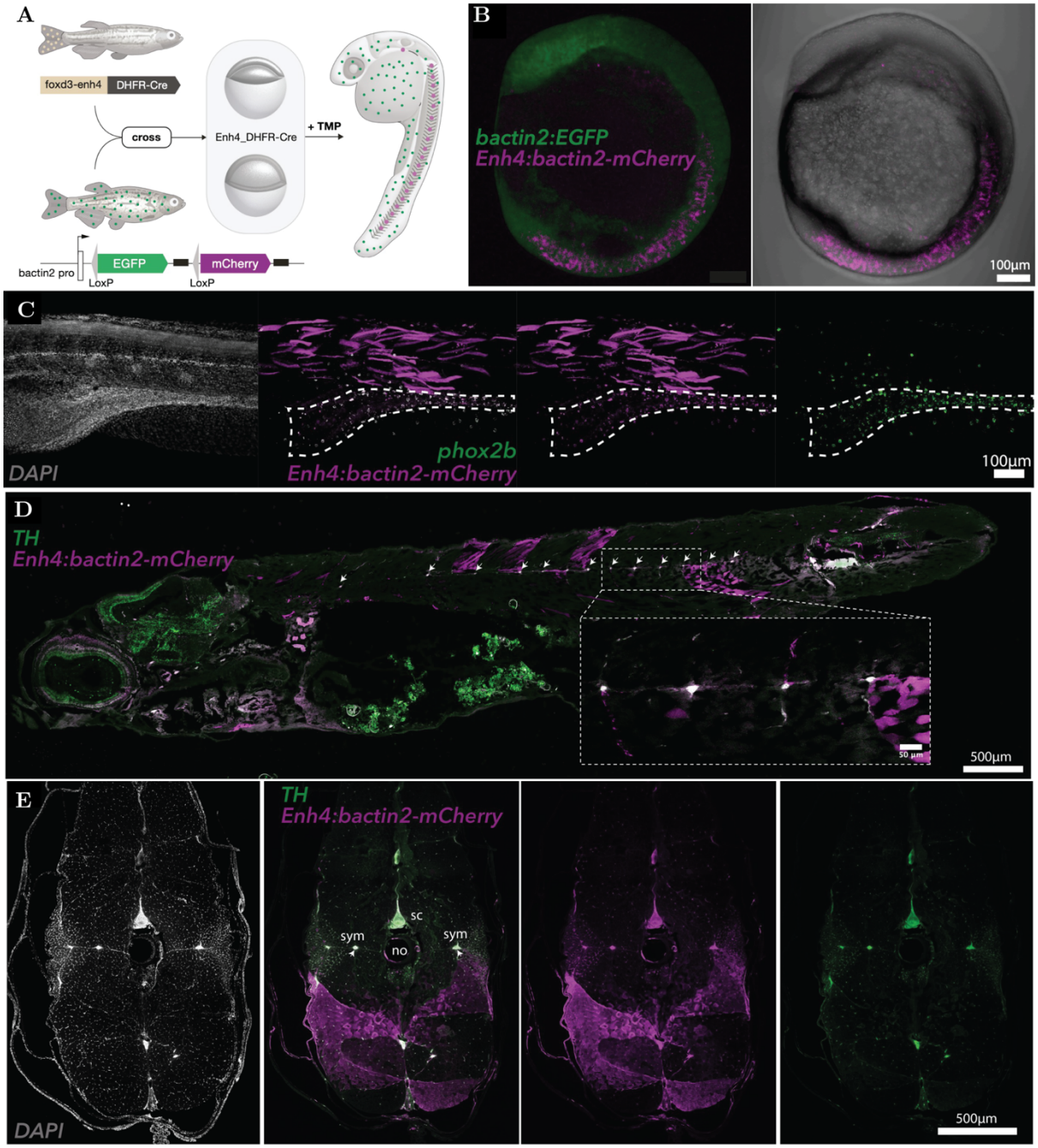

Figure 2 - NMP contributions to NC derivatives - (A) Transgenic zebrafish enables genetic lineage tracing of NMPs through constitutive mCherry labelling (Results). (B) Confocal image of migrating NMPs during zebrafish bud stage. (C) Whole mount immunofluorescence co-staining of Phox2b and mCherry in a 13 dpf fish. The outline marks the hindgut region and shows NMP contributions to Phox2b+ enteric neurons. (D) Sagittal section through a 35 dpf zebrafish larva co-stained for Th and mCherry shows NMP contributions to the sympathetic chain ganglia. The arrows point to the sympathetic chain ganglia. (E) Transverse section through a 41 dpf zebrafish larva co-stained for Th and mCherry shows NMP contributions to the spinal cord and the sympathetic chain ganglia on the lateral sides of the notochord. DHFR – Dihydroxyfolate reductase, sym – sympathetic ganglia, sc – spinal cord, no – notochord. Data from Lukoseviciute and Ateş 2025, under review. Credits: Seda Ateş-Kalkan, PhD.

1.6 Hypothesis and Aims

We hypothesize that NMPs are forming NC derivative cell types through an alternative peripheral neural-NC specific developmental trajectory with a distinct gene regulatory signature.

To address this hypothesis, we aim to achieve the following:

Aim 1 – **Lineage tracing and 10X 3' single-cell RNA-sequencing of NMPs in the zebrafish embryo and larva** to comprehensively profile NMP-derived cell fates

Aim 2 – **Integration and annotation of NMP derivatives** to uncover their transcriptomic identities

Aim 3 – **Analysis of NMP-derived neuronal populations using integrative analysis** to characterize NMP-derived neuronal cell types

1.7 Summary of Results

Using an approach combining genetic lineage tracing of NMPs and single-cell RNA-sequencing of NMP derivatives called Convert-seq, we demonstrate that NMPs give rise to diverse cell type derivatives in the zebrafish embryo. In addition to canonically known neuronal and mesodermal cell types, they also putatively contribute to the enteric and sympathetic nervous system and a Schwann cell precursor population.

Chapter 2 Materials and Methods

2.1 Zebrafish lines

The zebrafish lines used for this work are as follows: *Tg(FoxD3_ enh4:DHFR-Cre)*^{ox135} *Tg(ubb:loxP-mCherry-loxP-H2B-GFP)* were generated previously in the lab (Lukoseviciute & Ates et al. 2025, under review, credits: Seda Ateş-Kalkan, PhD) and the *Tg(ubb:loxP-EGFP-loxP-mCherry)*^{cz1701} by (Mosimann *et al.*, 2011). We also use multiome data (Hu *et al.*, 2024) from generated from two genetrap lines *Gt(ft110:FoxD3-Citrine)*^{ct110a} and *Gt(ft110:FoxD3-mCherry)*^{ct110aR} generated by (Hochgreb-Hägele and Bronner, 2013).

2.2 Zebrafish Husbandry

Animal handling and experiments were conducted in accordance with the protocols approved by the Stowers Institute for Medical Research Institutional Animal Care and Use Committee (IACUC) review board and in compliance with the guidelines outlined in the Guide for the Care and Use of Laboratory Animals (National Research Council Committee for the Update of the Guide for the and Use of Laboratory, 2011). Adult fish were cared for based on previously established protocols (Westerfield, 2000). Briefly, the adult fish were maintained in a 14-hour light and 10-hour dark cycle (with lights on from 7 am to 9 pm and lights off from 9 pm to 7 am). They were housed in a closed recirculating water system with temperatures in the range of 27-28.5°C, fed 3-4 times a day and maintained at around 5 fish per 1 L of water.

Males from *Tg(FoxD3_ enh4:DHFR-Cre)*^{ox135} line were crossed with females from *Tg(ubb:loxP-EGFP-loxP-mCherry)*^{cz1701} or *Tg(ubb:loxP-mCherry-loxP-H2B-GFP)* lines – the former for performing single-cell RNA-seq and the latter for single-nuclear RNA-seq. Individual or multiple pairs of fish were set up in breeding cages the previous afternoon divided by a transparent separator, which was pulled the following morning, the cages were placed on an incline and the fish were allowed to breed, followed by embryo collection. The embryos were raised in 0.5X E2 media (7.5 mM NaCl, 0.25 mM KCl, 0.5 mM MgSO4, 75 µM KH2PO4, 25 µM Na2HPO4, 0.5 mM CaCl2, 0.5 mg/L NaHCO3, pH = 7.4) at 28.5°C. Beyond 5 dpf, the larvae were fed with standard fry

feed (Westerfield, 2000). The staging of embryos was performed visually on Olympus dissecting stereomicroscopes and according to previously published methods (Kimmel *et al.*, 1995).

2.3 Lineage tracing of NMPs

Trimethoprim (TMP) was added to 0.5X E2 media at an effective concentration of minimum 5 µM to induce embryos at 30% epiboly stage. The TMP treatment was stopped at 1 dpf by washing and replacing the TMP-treated media with standard 0.5X E2 media to minimize TMP toxicity. The embryos were visually screened for positive mCherry fluorescence post-TMP treatment, collected separately and grown to the desired larval stage, followed by processing for single-cell RNA-sequencing. The embryos were given a media change every alternate day upto 5 dpf, and daily media changes along with feed after 5 dpf.

2.4 Embryo dissociation, cell isolation, and fluorescence-activated cell sorting (FACS)

Embryos at the desired stage were collected in 1.5 mL Eppendorf DNA low-binding tubes (30-50 embryos per tube depending on the stage), washed with PBS and the residual liquid discarded. 500 µL of 80 µg/mL effective concentration of Liberase™ (Roche) in PBS was added to the tubes and incubated for 25 min at 32°C. The digestion mix was pipetted intermittently (every 5 minutes) and pulverized with a sterile, autoclaved pestle at the 20-minute mark, to aid in mechanical dissociation of the embryos. The reaction was quenched by adding 400 µL 1% BSA in PBS and filtering through a 70-µm mini strainer (PluriSelect) by spinning at 500X *g* for 5 min at 4°C. Post-filtration, the samples were washed once with 500 µL 1% BSA in PBS, spun at 500X *g* for 5 min at 4°C and finally resuspended in 1 mL 5% BSA in PBS to prevent cells from clumping.

The single-cell suspension was stained with 1-3 µg/mL DAPI for selecting negatively against low-quality, dying cells. Unstained cells from wildtype, non-fluorescent embryos were used to set up a singlet gate for filtering single cells, followed by DAPI-stained cells to select for live cells. DAPI-stained GFP-positive but mCherry-negative cells were used as a positive control to visualise the difference in fluorescence as

compared to wildtype non-fluorescent cells. Finally, DAPI-negative live mCherry-positive cells were sorted into a DNA low-binding tube, coated with 1% BSA to prevent cell loss by sticking on the walls of the tube. FACS was performed on an S6 FACSymphony™ machine (BD Biosciences). To assess the cell quality and number, 5 µL of the cell suspension was added to equal volume of 0.4% Trypan Blue solution and mixed well. The mixture was then pipetted onto the haemocytometer chip C-Chip (iN CYTO) and the cell numbers were counted under a microscope.

2.5 Nuclei isolation and fluorescence-activated nuclei sorting

Embryos were collected and washed with PBS as mentioned above. After the residual liquid was discarded, the embryos were flash frozen in liquid nitrogen and stored at -80°C for later use. During dissociation, the embryos were kept on ice and 200 µL 0.5X lysis buffer (10 mM Tris-HCL (pH 7.4), 10 mM NaCl, 3 mM $MgCl_2$, 1% BSA, 0.05% IGEPAL and 0.05% Tween-20) was added into the tube. Using a sterile, autoclave pestle, the embryos were pulverized for 2-3 mins on ice and the reaction was quenched by adding 500 µL of wash buffer (10 mM Tris-HCL (pH 7.4), 10 mM NaCl, 3 mM $MgCl_2$, 1% BSA, 0.1% Tween-20) and mixing the suspension with a wide-bore pipette tip. The suspension was filtered through a 40-µm mini strainer (PluriSelect) and centrifuged at 500X *g* for 5 min at 4°C. Post-filtration, the samples were washed once with 500 µL of wash buffer and resuspended in 300 µL of 5% BSA to prevent clumping followed by another filtration with a 40-µm mini strainer. The single-nuclear suspension was stained with 1:1000 dilution of 7-AAD to select for nuclei. As described previously, unstained nuclei from wildtype, non-fluorescent embryos were used to set up a singlet gate, followed by the use of 7-AAD stained nuclei to select for nuclear events. Lastly, 7-AAD-positive mCherry-positive nuclei were sorted into a 1.5 mL DNA low-binding tube coated with 5% BSA to prevent nuclei loss by sticking to the walls of the tube. Nuclei were sorted using an S6 FACSymphony™ machine (BD Biosciences). The nuclear number, quality and morphology were assessed as described above.

2.6 10X Chromium 3' single-cell RNA-sequencing

Single-cell 3' RNA-seq libraries were prepared and sequenced by following the Chromium Next GEM Single Cell 3' v3.1 User Guide (Dual Index) (10X Genomics, CG000315). Briefly, sorted cells were loaded into the Chromium 10X Genomics Chip G, followed by loading gel beads from the Next GEM Single Cell 3' v3.1 Gel Beads (Cat. No. PN-2000164). The loaded chip was run on a Chromium iX controller for capturing single cells with 10X gel beads (GEM generation) and barcoding followed by an RT-PCR. After the RT reaction, the Gel Bead Emulsions (GEMs) were broken and first-strand of the cDNA recovered. After synthesizing cDNA, it was enzymatically fragmented and size-selected and P5 & P7 Illumina indexes, i5 & i7 sample indexes were added to form the final library. Libraries were quantified using Invitrogen Qubit™ (Cat. No.: Q32854) and Agilent TapeStation™ 4150. 2 nM 10X scRNA-seq libraries were sequenced on a NextSeq 2000 platform (Illumina) using NextSeq 2000 P3 v3/P2 X-LEAP (100 Cycles) (Cat.No. 20040559, 20100987) with 28 x 10 (i7) x 10 (i5) x 90 cycle number mode per sample. Each sample was sequenced to a sequencing depth of 300 million reads.

2.7 10X 3' single-cell/nuclear RNA-sequencing data pre-processing

Raw base call (BCL) files were demultiplexed and converted into a FASTQ format using cellranger mkfastq function (v8.0.1) (Zheng *et al.*, 2017). The FASTQ files were aligned to a customized transcriptome using the cellranger count function. The customized transcriptome was prepared using the cellranger mkref function. The customized FASTA and GTF files were prepared by appending the mCherry and H2B-GFP sequence to the GRCz11 Ensembl 110 reference transcriptome. The filtered feature barcode matrix output from cellranger was further used as input for cellbender remove-background function (Fleming *et al.*, 2023). The cellbender output of a hdf5 file was then read into R version 4.3.1 and analyzed using Seurat (v5) (Hao *et al.*, 2024). Upon reading in the hdf5 files, Seurat objects were created for each sample and filtered based on their gene expression profile. The scRNA-seq data was filtered for nFeature_RNA values between the range of 500 to 7500 and the percentage of mitochondrial reads to be below 5%. The snRNA-seq was filtered for nFeature_RNA values ranging from 100 to 3000 and the percentage of mitochondrial reads to be below 5%. Following this quality control, doublet cells were removed using the R package DoubletFinder (McGinnis *et al.*, 2019) by modelling homotypic doublets and filtering singlets.

2.8 Single-cell/nuclear RNA-sequencing clustering analyses

After pre-processing of the raw data, we performed clustering analysis and dimensional reduction to visualise the data. Raw counts were normalized using SCTransform normalization algorithm, which fits a negative binomial distribution to the data, then normalizes and scales the data, followed by selecting 2000 of the most highly variable genes (Hafemeister and Satija, 2019). Following this, we centred and scaled the data and performed dimensional reduction using principal component analysis (PCA). To decide upon the number of principal components (PCs) for further analysis, we used the ElbowPlot function. In most cases, due to the lack of a clear change in pattern of the data ('the elbow'), the minimum of first 50 PCs or the number of PCs corresponding to a standard deviation of 5% were selected for further analysis. Clustering was performed using the FindNeighbors and FindClusters functions with default settings, which uses the Louvain clustering algorithm to find transcriptomically distinct clusters. All samples were initially clustered at a resolution of 0.5, which was then varied based on the number of observable distinct clusters, which was usually achieved within the clustering resolution of 0.2 to 0.8. The marker genes of each cluster were identified using FindAllMarkers function with only.pos = TRUE argument and filtered for an adjusted p-value to be less than 0.05. The dataset was represented on a 2D plot using Uniform Manifold Approximation and Projection (UMAP) dimensional reduction using the RunUMAP function in Seurat.

2.9 Single-cell/nuclear RNA-sequencing data integration

To correct for technical batch effects among the different developmental stages, we utilized the Canonical Correlation Analyses (CCA) algorithm available in the Seurat package (Stuart *et al.*, 2019). We first pre-processed, clustered and dimensionally reduced the datasets using UMAP to visually inspect the structure of the UMAP and the differences in cell types between different stages. Upon observing broad concordance of the cell type clustering in different stages, we decided to proceed with using Seurat-CCA since it was unlikely to exhibit overcorrection errors in this scenario (Luecken *et al.*, 2022). We started by merging the datasets using the merge function

in base R. Since Seurat v5 stores each dataset in a separate layer inside the Seurat object, we use the Join Layers function to merge them into a single layer. Further, we split the RNA assay of the datasets based on their developmental stage and performed normalization using SCTransform by regressing out mitochondrial reads. After normalization and selection of highly variable genes, we performed dimensional reduction suign PCA to compute the top 100 PCs and select the top 50 PCs for further analysis. After this step, we first ran the FindNeighbors, FindClusters and RunUMAP functions on the unintegrated but merged and normalized data to visualize the extent of technical batch effects among different datasets. In case the datasets clustered based on their sequencing batch and not based on biological differences, we performed CCA integration using the IntegrateLayers function. Finally, we reran the FindNeighbor, FindClusters, and RunUMAP functions to generate a 2D UMAP plot of the data. Clusters were again visualized stage-wise using the group.by and split.by arguments of the DimPlot function to observe the overlap between different developmental stages.

2.10 Zebrahub reference dataset pre-processing

To annotate the cell types in our dataset, we used the Seurat FindTransferAnchors and TransferData functions. Prior to that, we prepared an annotated reference dataset from Zebrahub, the publicly available whole-embryo single-cell atlas in zebrafish (Lange *et al.*, 2023). For preparing the reference, we used the Zebrahub datasets that were closest to the developmental stages to be annotated in our dataset. To download the FASTQ files from the Sequence Read Archive (SRA) by NCBI, we used the fastq-dump from the sratoolkit module and input the SRA ids for the datasets on the command line which uses the bash programming language. Upon downloading the FASTQ files, we ran the cellranger count function on these datasets to generate the filtered feature barcode matrix as an output. We then used the hdf5 file of the filtered feature barcode matrices of each stage to import it into R using Seurat and created Seurat objects for each. The quality control metrics were the same as mentioned above, except we filtered for mitochondrial reads to be less than 10%. We then merged these datasets together and joined them into a single layer using the JoinLayers function.

To obtain the cell type annotations of the Zebrahub data and add it to the Seurat metadata, we downloaded the processed hdf5 anndata files available online through a Google Drive link provided on the Zebrahub website. After downloading the .h5ad files, they were read into Python using Scanpy (v1.11.0) read_h5ad function (Wolf *et al.*, 2018). The metadata was then exported into a CSV format using the Scanpy .to_csv function. The metadata CSV file was read into R, using the read.csv function

under the utils (v4.3.1) R package. The metadata of multiple stages was merged into a single data frame using the rbind function. The columns with the cell barcodes (cell_id) and the cell type annotations (zebrafish_anatomy_ontology_class) were subsetted and added to the metadata of the pre-processed reference in Seurat using the left_join function in the dplyr (v1.1.4) package to subset the matching cell barcodes. The dataset was then normalized using SCTransform without splitting the RNA assay into separate layers so that the single SCT assay can then be used by the CCA algorithm to find anchors and transfer annotations. Since anchor-based annotation transfer projects both the reference and query datasets onto a common PCA plot, it uses the single SCT assays from the reference and the query and as a result, further downstream processing of the reference including clustering and UMAP dimensional reduction is not required.

2.11 Single-cell/nuclear RNA-sequencing annotation transfer

After preparing the query dataset, we merged our stage-wise scRNA-seq and snRNA-seq datasets and joined them into a single layer as descrubed above. Thereafter, as mentioned for the Zebrahub reference, we normalized them using SCTransform and regressed out the mitochondrial reads to generate a single SCT assay object that would be used by the anchor-based annotation transfer algorithm. After normalization, we ran dimensional reduction using PCA and plotted an elbow plot to visualize and determine the number of PCs to be used for the annotation transfer. The FindTransferAnchors function was run using the first 60 PCs of the data and the k.anchor and k.score was increased to 10 and 50 respectively, which output an AnchorSet object. The AnchorSet object was then used to run the TransferData function using the first 60 PCs, which performs a k-nearest neighbours algorithm on each pair of anchors and outputs a Seurat object with the cell type annotation predictions based on the neighbourhood of the anchors. The predicted.id column containing the cell type annotation predictions and the predicted.id.score column containing the confidence of the predicted annotation were added to the metadata of the pre-processed Seurat object of the query dataset. For annotation of the clusters, the RNA assay of the query Seurat object was split stage-wise and renormalized using SCTransform. The clustering was performed at a high resolution of 2 to obtain the maximal number of distinct transcriptomic clusters followed by UMAP dimensional reduction. Upon clustering, we filtered the predicted.id column for a predicted.id.score

of greater than 0.7 and then assigned the most frequently occurring predicted.id to the entire cluster in a new column to obtain the cluster annotations.

2.12 Integrative analysis of enteric neurons using publicly available scRNA-seq dataset

The dataset characterizing *phox2bb*+ enteric neurons published by the Bronner lab (Li *et al.*, 2025) was used for the integrative analysis. The FASTQ files were downloaded from SRA, processed through Cellranger and pre-processed using the same criteria as mentioned above. The pre-processed Bronner datasets were then merged with our (TSS) datasets, split stage-wise, normalized using SCTransform and dimensionally reduced using PCA as described previously. The Bronner and TSS datasets were further integrated using Harmony (Korsunsky *et al.*, 2019). Harmony was first run on the PCA reduction of the merged Seurat object using the RunHarmony function and provided the variable having the stage information. The RunHarmony function uses the PCA embeddings and corrects them to align similar clusters across different stages. Further, we ran the IntegrateLayers function in Seurat with the integration.method=HarmonyIntegration as an argument, which then uses these corrected PCA embeddings to correct the expression values for each stage and outputs a new reduction which is stored in the object. The corrected Harmony reduction was then used for running the FindNeighbors, FindClusters, and RunUMAP functions. The clustering was performed using the Louvain clustering algorithm at a resolution of 2 as mentioned previously. The marker gene expression was visualized using the FeaturePlot, VlnPlot and DotPlot functions in Seurat.

Chapter 3 Results

3.1 Convert-seq – Single-cell RNA-sequencing of converted NMP derivatives

The first step to characterizing the GRN underlying NMP differentiation *in vivo*, is to comprehensively profile the NMP derivatives in the zebrafish embryo. To achieve global profiling of NMP derivatives in an unbiased manner, we leveraged 10X Chromium 3' single-cell transcriptomic sequencing in an approach called Convert-seq (Methods). Briefly, we crossed males from *Tg(foxd3_enh4:DHFR-Cre)*^{ox135} line with females from *Tg(ubb:loxP-EGFP-loxP-mCherry)*^{cz1701} line to derive embryos with a *foxd3_enh4:DHFR-Cre> ubb:loxP-EGFP-loxP-mCherry* genetic background. These embryos show constitutive EGFP expression throughout the entire body at all developmental stages. The embryos are treated with the antibiotic TMP at 30% epiboly, which marks the start of gastrulation and the NMP specification at the early embryonic tailbud. The TMP stabilizes the *DHFR* enzyme in the *foxd3_enh4+* NMPs where the *foxd3_enh4* is driving the expression of the *DHFR-Cre* construct. The *Cre* recombinase recombines at the *loxP* sites, activating constitutive expression of mCherry in the NMPs. Since the NMPs are constitutively labelled, this genetic lineage tracing approach enables us to study NMP derivatives at later stages during zebrafish development when the *foxd3_enh4+* NMP population has differentiated.

Further, we let these embryos grow to the desired larval stage followed by their dissociation into single cells (Methods) followed by Fluorescence Activated Cell Sorting (FACS) of mCherry+ cells. We performed 10X Chromium 3' single-cell RNA-sequencing on the mCherry+ cells to infer the transcriptomic identities of the NMP derivatives. The sequencing data was run through the cellranger pipeline by 10X Genomics to recover the single-cell gene expression matrix and the data was filtered for low-quality cells (Figure 3A). To confirm if we isolate bonafide NMP populations through our FACS gating strategy, we leveraged previously available global *foxd3+* 10X single-cell multiome (snRNA-seq and scATAC-seq) dataset in the lab (Hu *et al.*, 2024). We generated scRNA-seq datasets at corresponding stages of the single-cell multiome dataset, namely 90% epiboly or bud-stage to 4 somite stage (ss), 8 ss to 12 ss, 14 ss to 16 ss and 18 ss to 22 ss. We utilized the RNA component of the multiome dataset and our Convert-seq data to perform integrative analysis of these cell populations using Canonical Correlation Analysis (CCA) algorithm available in the

Seurat package (Stuart *et al.*, 2019). CCA projects the datasets to be integrated onto a common PCA plot and performs k-nearest neighbours clustering to identify pairs of transcriptomically similar cells called anchors. It then scores and filters these anchor pairs and uses them to correct the normalized gene expression values and maps all the corrected gene expression values in a dimensionally reduced, batch corrected space.

Upon integration, we expected transcriptomically similar cells to cluster together onto the dimensional reduction plot, which is a UMAP in our case. Since the *foxd3_enh4+* NMPs express *foxd3* at attenuated levels in the posterior region of the embryo, we expected our Convert-seq data to be a subset of the *foxd3+* multiome dataset. Indeed, we noted significant co-clustering of the Convert-seq data with the multiome dataset (Figure 3B). Our Convert-seq cells were broadly distributed across multiple clusters of the multiome dataset at all early embryonic stages throughout somitogenesis, which indicates that the Convert-seq approach is able to capture the mCherry-labelled NMP cell population. Upon overlaying the Convert-seq and multiome datasets, we observed that our Convert-seq data, represented in grey, primarily clustered at the top of the UMAP plot as shown in the grey inset, indicating the posterior domain of *foxd3* expression in the zebrafish embryo. Additionally, using our constitutive labelling approach, we were also able to recover novel and possibly transient *foxd3+* cell populations as shown in the red outline, which were not captured in the multiome dataset which uses the endogenously-tagged *foxd3* expression to profile these cells (Figure 3C).

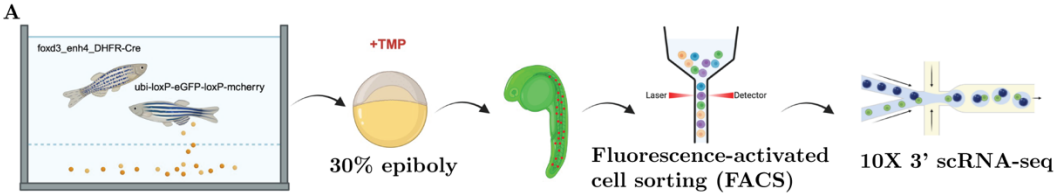
A
foxd3_enh4_DHFR-Cre
ubi-loxP-eGFP-loxP-mcherry
+TMP
30% epiboly
Laser
Detector
Fluorescence-activated
cell sorting (FACS)
10X 3' scRNA-seq

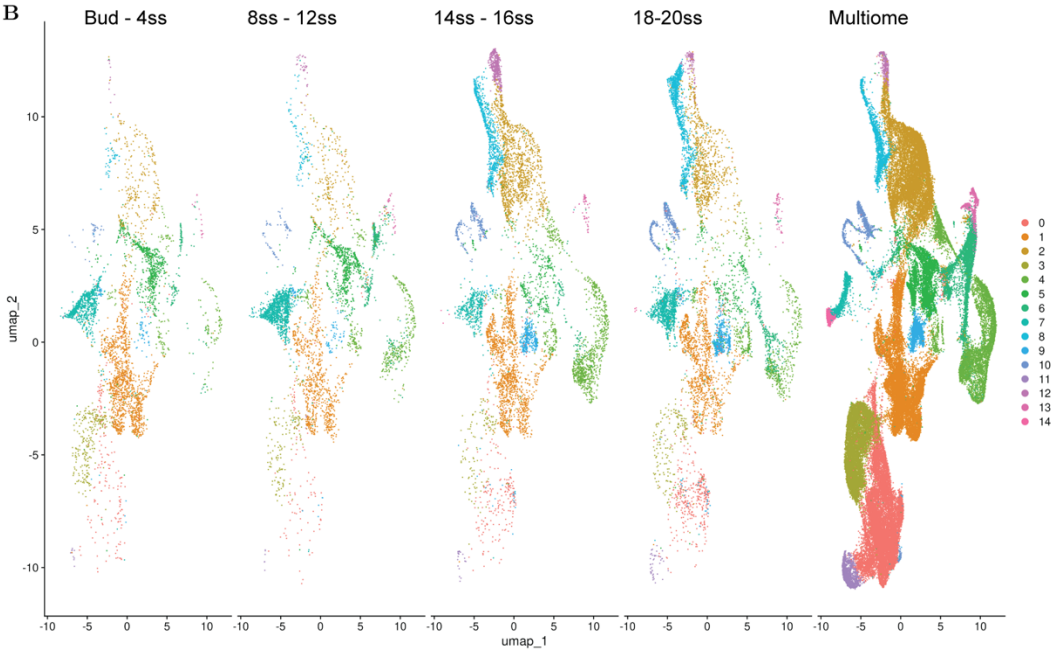
B
Bud - 4ss
8ss - 12ss
14ss - 16ss
18-20ss
Multiome
umap_2
umap_1
0
1
2
3
4
5
6
7
8
9
10
11
12
13
14

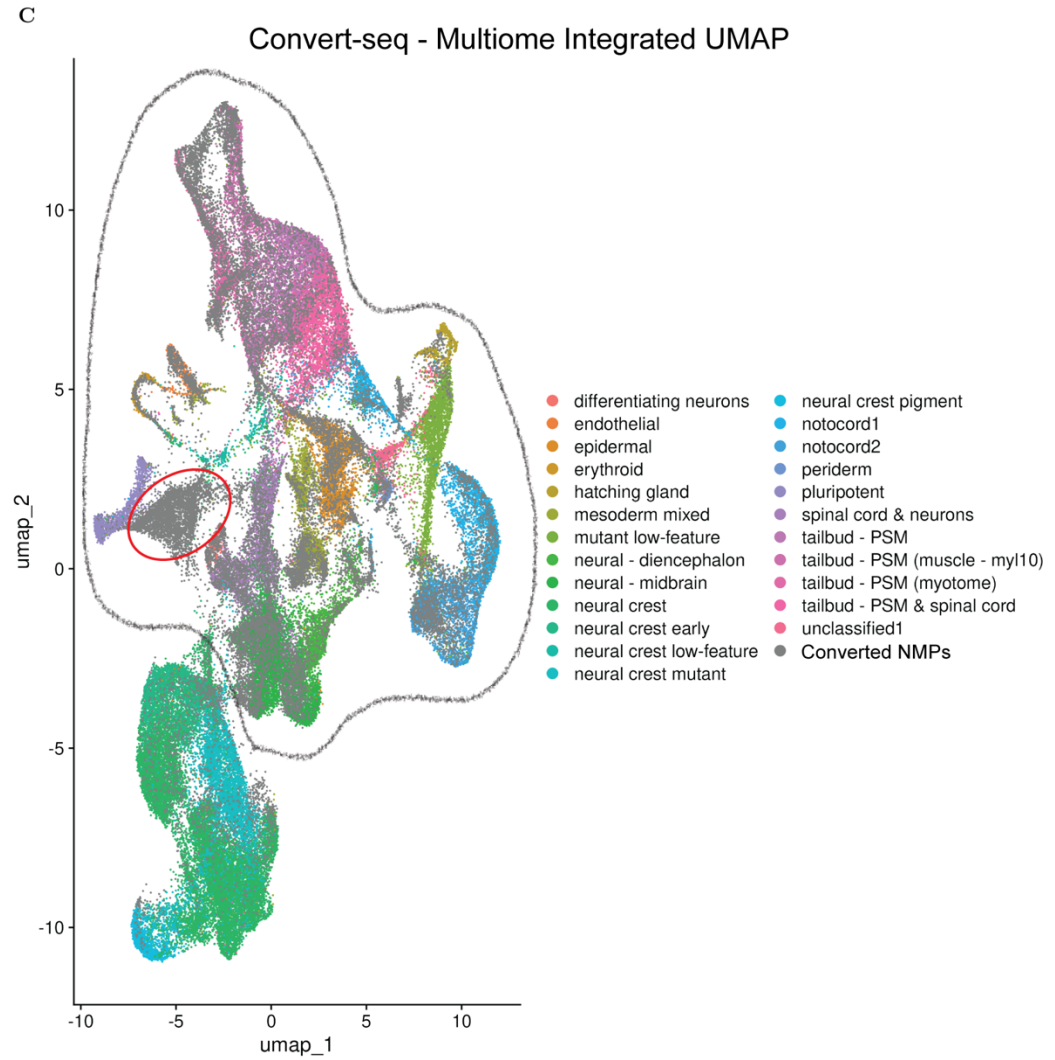
C
Convert-seq - Multiome Integrated UMAP
umap_2
umap_1
differentiating neurons
endothelial
epidermal
erythroid
hatching gland
mesoderm mixed
mutant low-feature
neural - diencephalon
neural - midbrain
neural crest
neural crest early
neural crest low-feature
neural crest mutant
neural crest pigment
notocord1
notocord2
periderm
pluripotent
spinal cord & neurons
tailbud - PSM
tailbud - PSM (muscle - myl10)
tailbud - PSM (myotome)
tailbud - PSM & spinal cord
unclassified1
Converted NMPs

Figure 3 – Convert-seq – Single-cell RNA-sequencing of converted NMPs. (A) Convert-seq workflow schematic. Credits: Seda Ateş-Kalkan, PhD. (B) Convert-seq – multiome integrated dataset, split by sample – Convert-seq dataset co-clustering with the multiome and broadly distributed across multiple clusters in the multiome. (C) Convert-seq – multiome integrated dataset, overlayed – Convert-seq cells (represented in grey) distributed primarily in the upper parts of the UMAP (marked by grey boundary) indicating the posterior domain of *foxd3* expression in the zebrafish embryo. The red outline shows a novel NMP population recovered through Convert-seq.

3.2 Single-cell RNA-sequencing of NMP derivatives through multiple zebrafish larval stages

After validating the Convert-seq approach using the *foxd3+* single-cell multiome, we decided to perform Convert-seq to profile NMP derivatives at the larval stages of the zebrafish. To capture crucial developmental dynamics like the migration and differentiation of the ENS and differentiation of other posterior NC-derived populations, we decided to perform Convert-seq at a wide range of developmental stages which include 2, 4, 6, 8, and 10 days post-fertilization (dpf). Since each of the developmental stages were sequenced in different batches, we performed batch effect correction on these datasets by integrating them into a single dataset using the CCA algorithm as mentioned previously.

Upon batch effect correction and clustering of the data to identify cell types based on transcriptomic similarity, we observed 28 distinct clusters (0 - 27) of NMP derivatives which suggest NMPs contribute to a wide range of cell type derivatives in the zebrafish larva (Figure 4C). We also observed that the CCA algorithm was able to ameliorate the technical batch effects effectively while retaining the biological effects in the dataset, as seen by the effective co-clustering of cell populations profiled at different developmental stages in the post-integration UMAP (Figure 4A,B). We also observed mCherry expression at varying levels throughout all the clusters of our Convert-seq dataset. We also noted that mCherry expression is not observed uniformly in all cells of the dataset due as a technical artifact of the process of random selection and a relatively high dropout rate of the 10X single-cell sequencing technology (Figure 4D).

To further characterize and annotate our dataset, we looked at the expression of important marker genes unique to particular cell types. For example, *phox2bb* is a crucial transcription factor involved in the development of the ENS from the vagal NC in vertebrate embryos. As mentioned previously, the zebrafish ENS proliferates and differentiates, forming a mature functional system by 5 dpf, corresponding to the opening of the mouth and initiation of feeding in zebrafish larvae. As a result, studies

have previously observed an increase in the *phox2bb+* enteric progenitors and neurons colonizing the gut as the larva develops.

As previous data from our lab suggests NMP contributions to the ENS in zebrafish larvae, we checked *phox2bb* expression across different developmental stages using our Convert-seq atlas. However, we observed a consistent decrease in the *phox2bb* expression as the larva develops. Although we had recovered distinct number of cells per developmental stage, it was surprising to see the decrease in the maximum expression level of *phox2bb* at higher developmental stages (Figure 4E).

We hypothesized that this decrease in the level of *phox2bb* expression is a technical artifact of the cell dissociation protocol. We observed that as the larvae develop, it becomes tougher to dissociate them effectively due to the formation of a compact extracellular matrix. We also observed a concomitant decrease in quality of the isolated cells under the microscope as the developmental stage of the larvae increased. As the neuronal progenitors differentiate into neuroblasts and further mature, these neurons form synaptic connections with other neurons. The loss of these synaptic connections in addition to the microfluidic-based FACS and 10X sequencing procedure might lead to the apoptosis of these cells leading to their dropout during the sequencing stages or the quality control stages.

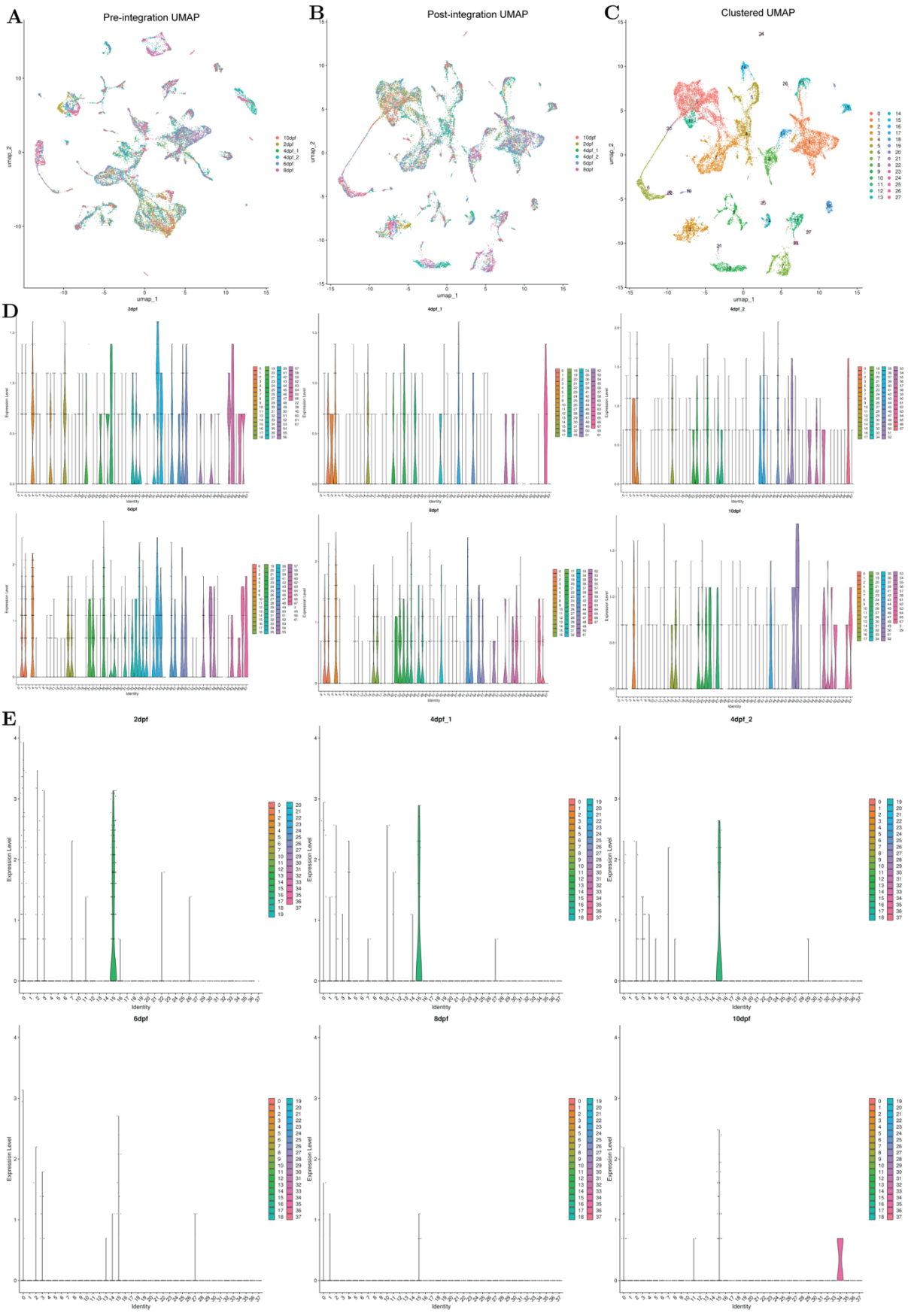

Figure 4 – Larval stage Convert-seq data integration – (A) Merged unintegrated UMAP of larval stages 2dpf – 10 dpf shows developmental stages clustering on the basis of technical batch effects. (B) UMAP post-integration shows effective removal of technical batch effects and co-clustering of developmental stages. (C) UMAP with the 28 clusters comprising of 25000 cells upon Louvain clustering at a resolution of 0.5, resolving transcriptionally distinct

clusters in the dataset. (D) Violin Plots for visualizing mCherry expression across developmental stages in the cells captured in Convert-seq show broad expression of mCherry across multiple clusters, supporting the validity of the Convert-seq approach. (E) Violin Plots for visualizing *phox2bb* expression across developmental stages shows a consistent decrease in the levels of expression and number of clusters showing expression which is contrary to findings in the literature.

3.3 Nuclear labelling improves capture of neuronal NMP derivatives

To solve the aforementioned limitation of our mCherry labelling approach, we devised a strategy to label the nuclei of the NMP derivatives instead of labelling cells. Single-nuclear RNA sequencing has emerged as a method for the efficient transcriptomic profiling of cell types that have been previously intractable to scRNA-seq protocols due to their multinucleate nature, cell adhesive properties, sensitivity to dissociation procedures, among other biological and technical reasons (Bakken *et al.*, 2018; Waag and Bohacek, 2023). Typical nuclear isolation protocols rely on dissociation of the sample into single-cell suspension followed by cell lysis and isolation of nuclei. However, the NMP derivatives represent a small fraction of the larval cell populations (<1%) which further decreases as the larva grows. As a result, we decided to generate a transgenic zebrafish line which enables genetic lineage tracing by nuclear labelling of the NMP derivatives.

To that effect, we established a transgenic zebrafish line, *Tg(ubb:loxP-mCherry-loxP-H2B-GFP)*, which is based on the same lineage tracing principle as the *Tg(ubb:loxP-EGFP-loxP-mCherry)*^{cz1701} line but effectively labels NMP nuclei instead of cells when crossed with males from the *foxd3_enh4:DHFR-Cre* genetic background. Confocal imaging of the larvae showed clear and distinct nuclear labelling with H2B-GFP (Figure 5A). The TMP treatment for the nuclear labelling is performed in an identical manner as mentioned previously, followed by dissociation and isolation of nuclei from the larvae.

Using the nuclear labelling transgenic line, we standardized the nuclei isolation protocol and performed snRNA-seq on 6 dpf zebrafish larvae. Due to the low RNA content of the nuclei compared to cellular RNA content, we observed significant differences in the number of Unique Molecular Identifiers (UMIs) recovered from the nuclear RNA-seq as compared to the cellular RNA-seq. As a result, when we compared the differences in cell type composition between the two datasets, we observed almost exclusive clustering of both datasets due to the sheer difference in the depth of their

transcriptomic profiling (Figure 5B). To remove these technical differences, we repeated the batch correction using CCA as mentioned previously and reclustered the dataset. We observed marked improvement in the co-clustering of the cell types. While the nuclear data is distributed through most clusters, we also noted that the nuclear data is enriched for certain cell types that are missing in our cellular data (Figure 5C).

To further confirm the identity of the nuclear enriched population, we performed annotation transfer using Seurat, which uses an anchor-based strategy to map the reference and query datasets onto a common PCA plot and performs k-nearest neighbour clustering algorithm to provide prediction scores and identities for the cell types in the query dataset (Stuart *et al.*, 2019). We utilized a previously published whole embryo scRNA-seq atlas of zebrafish called Zebrahub as the reference dataset (Lange *et al.*, 2023). Upon transferring annotations from Zebrahub, we observed that the cell populations enriched in the nuclear data are neuronal populations, based on their predicted annotations and marker gene expression (Figure 5D). However, we also noticed that although we recover a greater proportion of neuronal populations than scRNA-seq, the expression of marker genes in the nuclear data is appreciably lower than the cellular data due to the difference in UMI numbers recovered from both datasets.

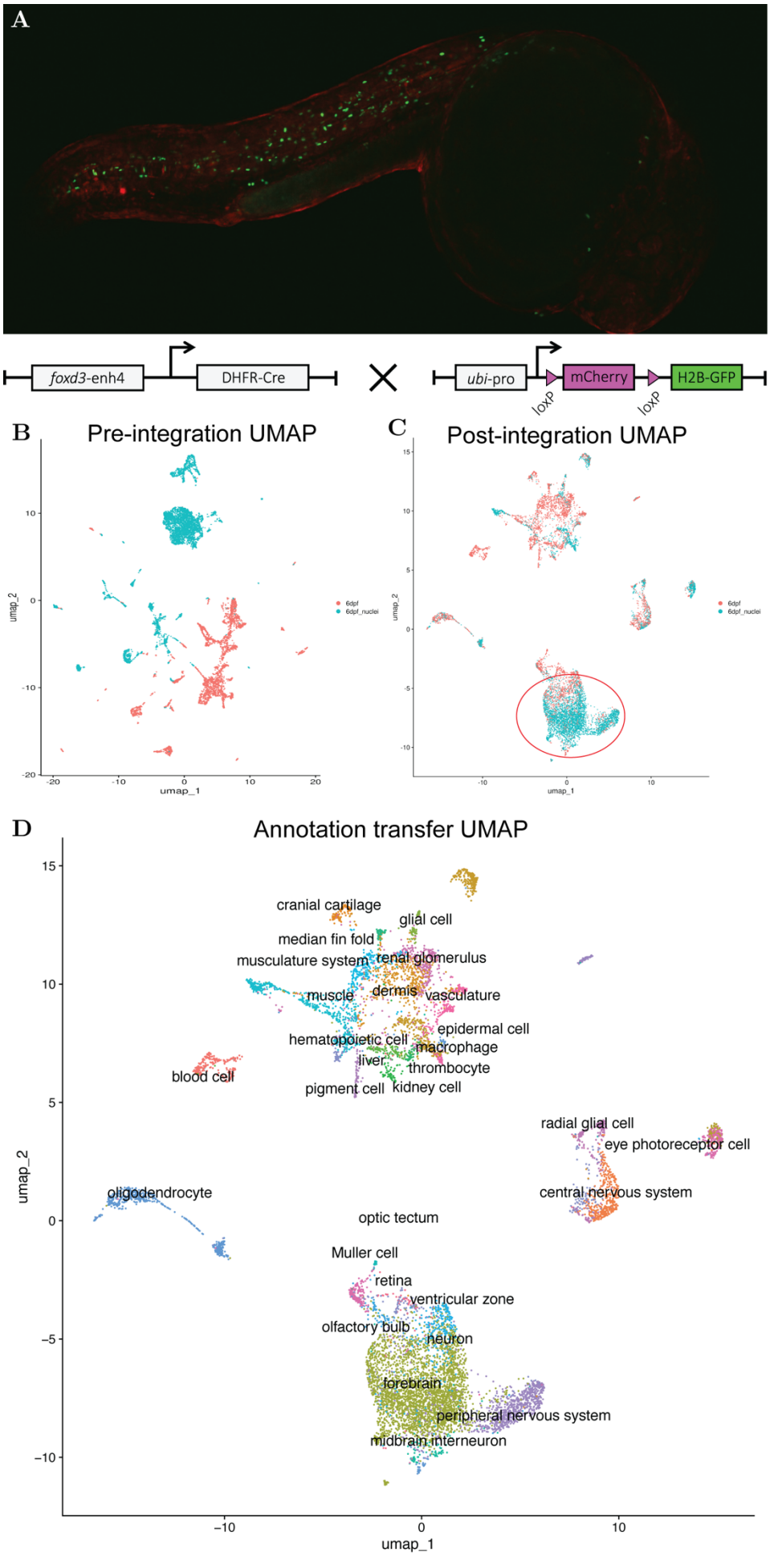
A
foxd3-enh4
DHFR-Cre
ubi-pro
mCherry
H2B-GFP
loxP
loxP
B
Pre-integration UMAP
C
Post-integration UMAP
umap_1
umap_2
6dpf
6dpf_nuclei
D
Annotation transfer UMAP
cranial cartilage
glial cell
median fin fold
musculature system
renal glomerulus
muscle
dermis
vasculature
epidermal cell
hematopoietic cell
macrophage
liver
thrombocyte
blood cell
pigment cell
kidney cell
radial glial cell
eye photoreceptor cell
central nervous system
oligodendrocyte
optic tectum
Muller cell
retina
ventricular zone
olfactory bulb
neuron
forebrain
peripheral nervous system
midbrain interneuron

Figure 5 – Genetic lineage tracing using constitutive nuclear labelling – (A) Confocal imaging of a transgenic 1 dpf zebrafish embryo (*foxd3-enh4::*DHFR-Cre>ubi::loxP-mCherry-loxp-H2B-GFP) expressing H2B-GFP in the NMP nuclei in the trunk. The AP axis of the embryo is directed in a right-left manner. The bottom panel represents a schematic for the nuclear labelling approach. (B) Merged unintegrated UMAP shows significant technical batch effects between scRNA-seq and snRNA-seq in NMP derivatives of 6 dpf zebrafish larvae, due to differences is amount of mRNA recovered from nuclei vs. cells. (C) Integration using CCA is able to correct for the technical batch effects and shows co-clustering of similar cell types in nuclear and cellular datasets. The red outline shows significant enrichment of neuronal populations in the nuclear data as compared to the cellular data. (D) Annotated UMAP with annotations transferred from the Zebrahub reference dataset. The bottom part of the UMAP shows the neuronal populations contributed by the NMPs.

3.4 A time-resolved comprehensive transcriptomic atlas of NMP derivatives in the zebrafish larva

To supplement the previously sequenced scRNA-seq data, we performed snRNA-seq on 6 dpf (as described in the previous section, Figure 5) and 12 dpf larval stages to account for neuronal populations that might be missing from our cellular data. The 2 dpf till 10 dpf scRNA-seq datasets were integrated with the 6 dpf and 12 dpf snRNA-seq using CCA and represented on a UMAP plot (Figure 6A). We also transferred annotations from Zebrahub and obtained predicted cell type annotations along with a predicted score. We clustered the dataset at high resolution to recover maximal clusters with distinct transcriptomic signature, followed by filtering the predicted annotations with a confidence value of 0.7 or above and assigned the most frequently occurring annotations to the cluster. Using this approach, we were able to uncover the identities of a broad range of NMP derivatives in the zebrafish larva.

We uncover a significant number of novel NMP derivatives previously unknown in the literature. While we obtain previously well characterized mesodermal derivative cell types like skeletal muscle cells, myoblast, muscle tissue, and hematopoietic cells among others; we also uncover novel contributions like a conspicuous population of glia, peripheral and central nervous system and retinal cell types. Among the mesenchymal cell types, we also found several clusters like median fin fold, cranial cartilage and head mesenchyme, which were believed to completely derive from the cranial NC, further bolstering our hypothesis (Figure 6C). Unique cell populations were also verified using the expression of top cluster marker genes with the highest fold-change and specificity to the particular cluster. For example, the expression of a canonical RNA binding protein gene *elavl3* & *elavl4* in the neural (neuronal and glial) cell types, etc (Figure 6D). For the purpose of this study, we specifically focused on the neuronal cell types that were canonically believed to arise from the posterior NC populations like the vagal and trunk NC but based on our immunofluorescence staining data are seen to have

some NMP contributions (Figure 2). To investigate this, we decided to perform integrative analysis using previously published scRNA-seq datasets of NC-derived PNS populations to discover and characterize novel cell types based on shared transcriptomic signatures.

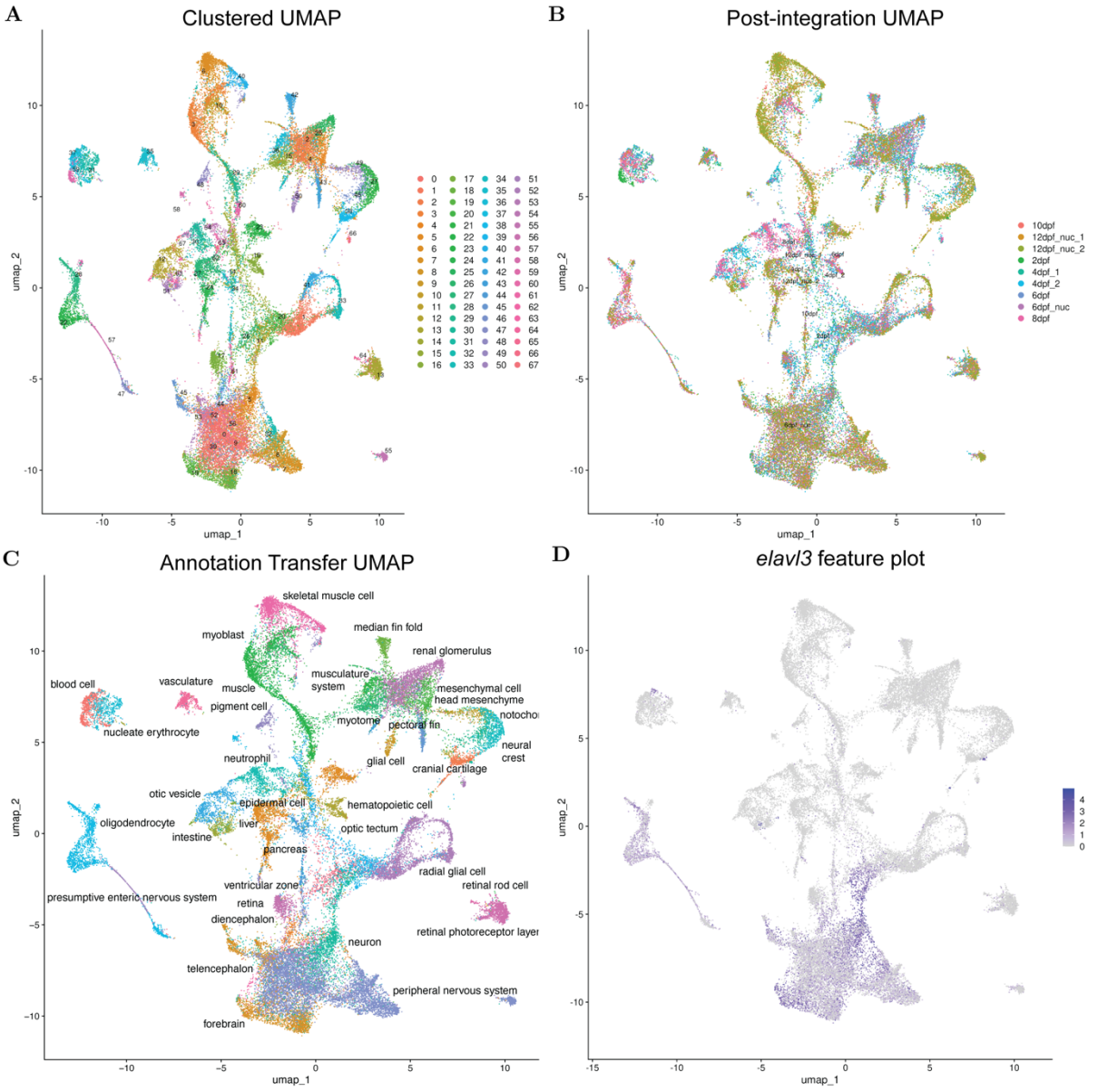

Figure 6 – Comprehensive single-cell atlas of NMP derivatives in the zebrafish larva – (A) UMAP showing the clustered dataset of 41410 cells and nuclei processed after including 6 and 12 dpf scRNA-seq data to the previous 2dpf – 10dpf scRNA-seq data. 68 clusters were obtained after performing Louvain clustering at a high resolution of 2. (B) UMAP showing diverse developmental stages from 2 dpf till 12 dpf integrated using CCA for batch effect removal. (C) Annotated UMAP with annotations transferred from a reference Zebrahub dataset. NMPs contribute to a wide range of diverse developmental derivative cell types in the zebrafish embryos, including mesenchymal and neuronal derivatives previously considered to be NC-derived. (D) Feature plot showing expression of a neural specific RNA-binding protein *elavl3* which is used as a marker for studying neuronal cell types.

3.5 Integrative analysis of enteric neuronal cell types using previously published datasets

Based on our immunofluorescence staining data suggesting NMP contributions to the posterior part of the enteric nervous system (ENS) (Figure 2) and based on expression of *phox2bb* in our dataset (Figure 4E), we hypothesized that our Convert-seq approach has captured the enteric neuronal populations formed by NMPs. As a result, we aimed to characterize the enteric neuronal cell types using integrative analysis with previously published datasets. There have been only a few studies which attempt to characterize the cell type diversity in the gut of the larval zebrafish using single-cell transcriptomic methods. One of the major studies, Li et al. 2025, has used a transgenic reporter line *Tg(Phox2bb:mNeonGreen)* to lineage trace *phox2bb+* enteric neuronal progenitors, neuroblasts and neurons and profiled them using scRNA-seq from 2dpf till 6dpf (Li *et al.*, 2025). This developmental window captures the dynamics of the ENS from the vagal NC cells entering the gut to the final establishment of the complete neuronal cell type diversity.

Due to the vast technical and biological difference between the Li et al. 2025 data (hereafter referred as the Bronner dataset) and our 2 dpf till 12 dpf Convert-seq data (referred to as TSS dataset), we performed integration and batch effect correction using Harmony (Korsunsky *et al.*, 2019). Several benchmarking studies have demonstrated that Harmony shows higher performance at handling non-linear batch effects and on complex integration tasks, while the CCA algorithm in Seurat can often lead to overcorrection and loss of biological heterogeneity (Tran *et al.*, 2020; Luecken *et al.*, 2022; Heumos *et al.*, 2023; Song *et al.*, 2023). Similar to our previous approach, upon integration we clustered the data at high resolution to uncover maximal cell type heterogeneity and obtained 68 clusters (0-67) (Figure 7A).

While most clusters are composed of cells exclusively from one of the datasets, visually we found two major domains of co-clustering (Figure 7B). Based on marker gene expression, we could observe that the upper parts of the UMAP plot show co-clustering between vagal NC-derived enteric neuron progenitors from the Bronner data with the mesenchymal cranial NC-like derivatives from the TSS data, indicating the actively proliferating multipotent state of the NC progenitors (Figure 7B,D). On the contrary, the lower parts of the UMAP show co-clustering between mature neurons from the Bronner data with PNS clusters from the TSS data, suggesting possible convergence of neuronal cell fates in the gut of the embryo (Figure 7B,C). However, due to the vast

heterogeneity of the dataset, we were unable to resolve specific enteric neuron cell types as demonstrated by Li et al. (Li *et al.*, 2025).

Therefore, to especially focus on the mature neuronal populations in the dataset, we subsetted the dataset using expression of neural-specific RNA-binding protein gene *elavl3* & *elavl4*, and the expression of a synaptic protein synaptotagmin 25 a/b, *snap25a* & *snap25b* (Figure 7C). The expression of these markers specifically allowed for the selection of neuroblasts and mature neurons and glia, thereby increasing the resolution of clustering in the dataset. Upon reclustering, we were able to recapitulate the branching developmental trajectory of the enteric neurons as shown by Li et al (Figure 7E). Unsurprisingly, we observed almost exclusive clustering of Bronner and TSS datasets, which is concordant with the distinct biological nature of the two datasets; the Bronner data specifically profiles the vagal NC-derived ENS while the TSS dataset profiles NMP derivatives. However, we did observe co-clustering in a few clusters of the dataset, specifically clusters 46 and 15 (C46 and C15), which represent putative enteric neurons formed by the contributions from the vagal NC and NMPs (Figure 7F).

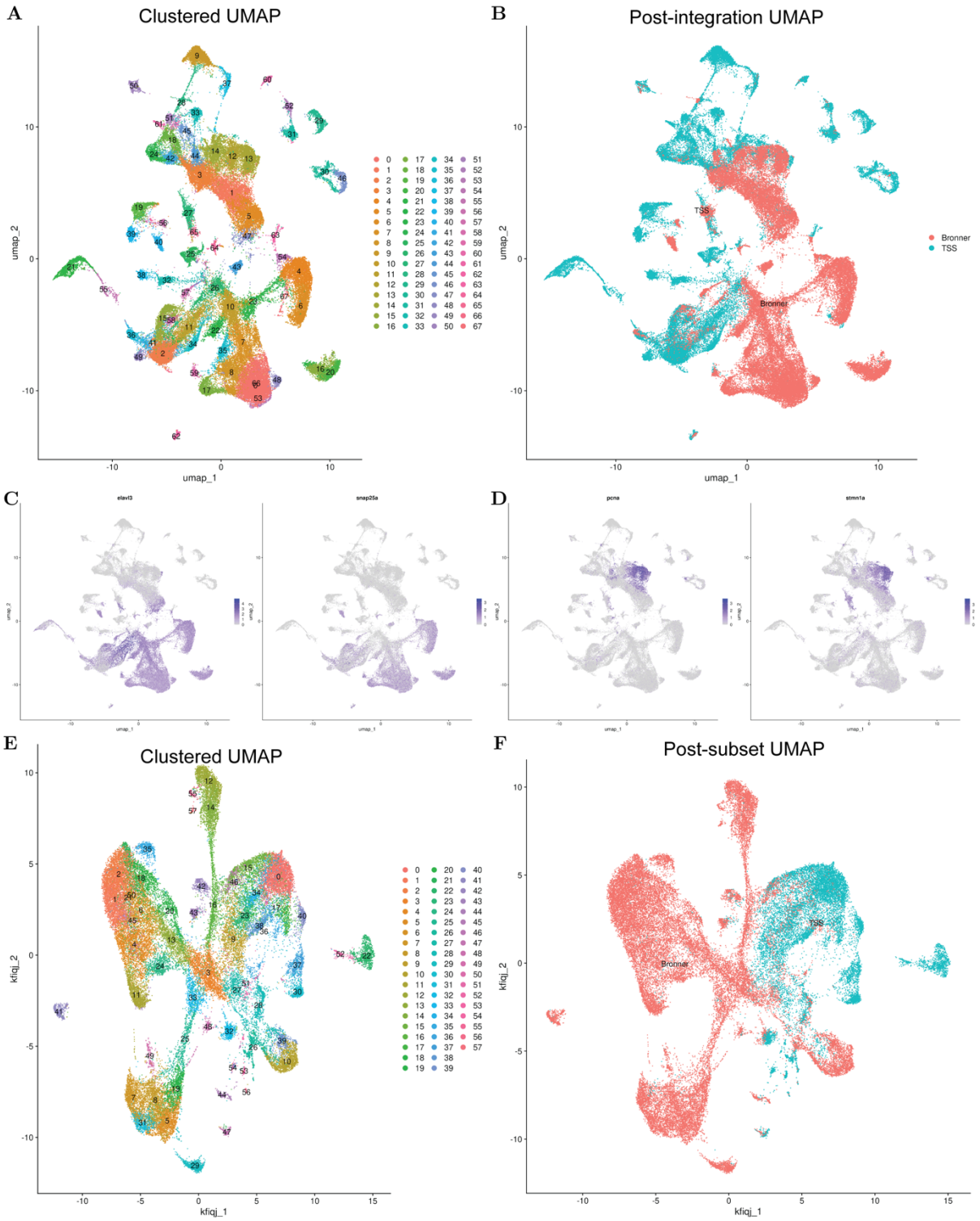

Figure 7 – Integrative analysis using enteric nervous system scRNA-seq dataset – (A) Integrated UMAP showing a clustered dataset comprising of 91517 cells and nuclei, of which 50107 cells belong to the Bronner dataset. (B) Harmony integrated UMAP which shows the limited co-clustering of Bronner and TSS datasets. The upper parts of the UMAP show co-clustering between progenitor populations while the bottom parts show co-clustering between mature neuronal populations. (C, D) Feature plots of *elavl3, snap25a, pcna, stmn1a*. *pcna* and *stmn1a* expression support their actively cycling progenitor populations, while *elavl3* and *snap25a* expression marks mature neurons. (E) UMAP representing clusters after subsetting and reclustering of mature neural cell types in the integrated dataset, the subset consisting of 51784 cells and nuclei, among which only 15390 cells and nuclei belong to the TSS dataset. (F) UMAP representing batch information of the two datasets, shows that while most of the dataset

maintains exclusive clustering, there exist certain domains of co-clustering which indicate presence of transcriptionally similar neuronal populations between two datasets.

3.6 Marker gene expression analysis to uncover identity of NMP-derived enteric neurons

To delineate the identity of the enteric neurons putatively formed by the convergence of vagal NC and NMP cell fates, we referred to the published studies that have characterized the ENS cell type diversity and checked for the expression of candidate marker genes. While there is limited literature on the zebrafish ENS, several studies characterizing the mouse ENS provide critical insights into the process and evolutionarily conserved genes that are required for ENS development.

First, we could observe expression of *paired like homeobox* transcription factors, *phox2bb* and *phox2a*, that are known to play a critical role in vagal NC-derived ENS development in C46 and in lesser abundance in C15 (Figure 8B). However, some studies have also discovered certain subpopulations of the ENS which do not express *phox2bb* (Kuil *et al.*, 2023). Second, we also found the expression of nerve growth factor receptor*, ngfra,* and the glial-derived neurotrophic factor (GDNF) receptor *ret*, in C46 and C15 (Figure 8B), the expression of which makes the enteric neuron progenitors receptive to the attractive GDNF signalling ligand causing the cells to migrate into the gut (Shepherd *et al.*, 2001). Third, C46 and C15 also express transcription factors involved in the specification of enteric neuron subpopulations like *pbx3b* and *onecut1* (Figure 8B).

Interestingly, the Li et al. 2025 study describes *onecut1* as a crucial player in specifying the identity of a unique population of enteric neurons expressing the neurotransmitter galanin (*gal*), which have a distinct transcriptomic identity and localization in the zebrafish gut (Li *et al.*, 2025). Consistent with their claims, the Bronner dataset also shows two clusters, C43 and C46, as *onecut1+* neurons, however, only C43 express *gal*. This suggests the possibility that *onecut1* might play a role in specifying different neuronal subpopulations, each with a distinct neurotransmitter identity and consequently a distinct functional role.

Studies in zebrafish and mice models have demonstrated the presence of heterogeneity of neuronal populations along the length of the gut, largely owing to the differences in rhythmicity of peristaltic muscle contractions (Morarach *et al.*, 2021; Li *et al.*, 2025). Since our data shows NMP contributions particularly to the posterior parts of the

ENS, we expect NMP-derived neurons to have a transcriptomic identity distinct from the remainder of enteric neurons. Another study in zebrafish found the presence of *phox2bb*- neurons in the gut which were glutamatergic in nature, suggested by expression of *vglut2* (Kuil et al., 2023). Since the TSS dataset shows sparse expression of *phox2bb*, we hypothesized that NMPs might contribute to this *phox2bb*- glutamatergic neuronal population.

Surprisingly, glutamate receptor subunits, *gria3, grid1a and* grid2, all show substantial expression in C46 and C15, providing support for our hypothesis (Figure 8C). While there is a lack of literature that has studied the role of glutamatergic neurons in the zebrafish gut, the mouse literature provides several crucial insights into the role of glutamatergic neurons in the mammalian gut (Kirchgessner, 2001; Filpa *et al.*, 2016; Swaminathan *et al.*, 2019). Based on this, we further checked for the expression of cholinergic markers, *slc18a3a* & *chata*, both of which show expression in C46 and C15 and are found to colocalize with glutamate markers in the mice gut. We also found expression of other excitatory neurotransmitters like Calbindin1 (*calb1*), which is concordant with the findings in mice ENS studies (Figure 8C).

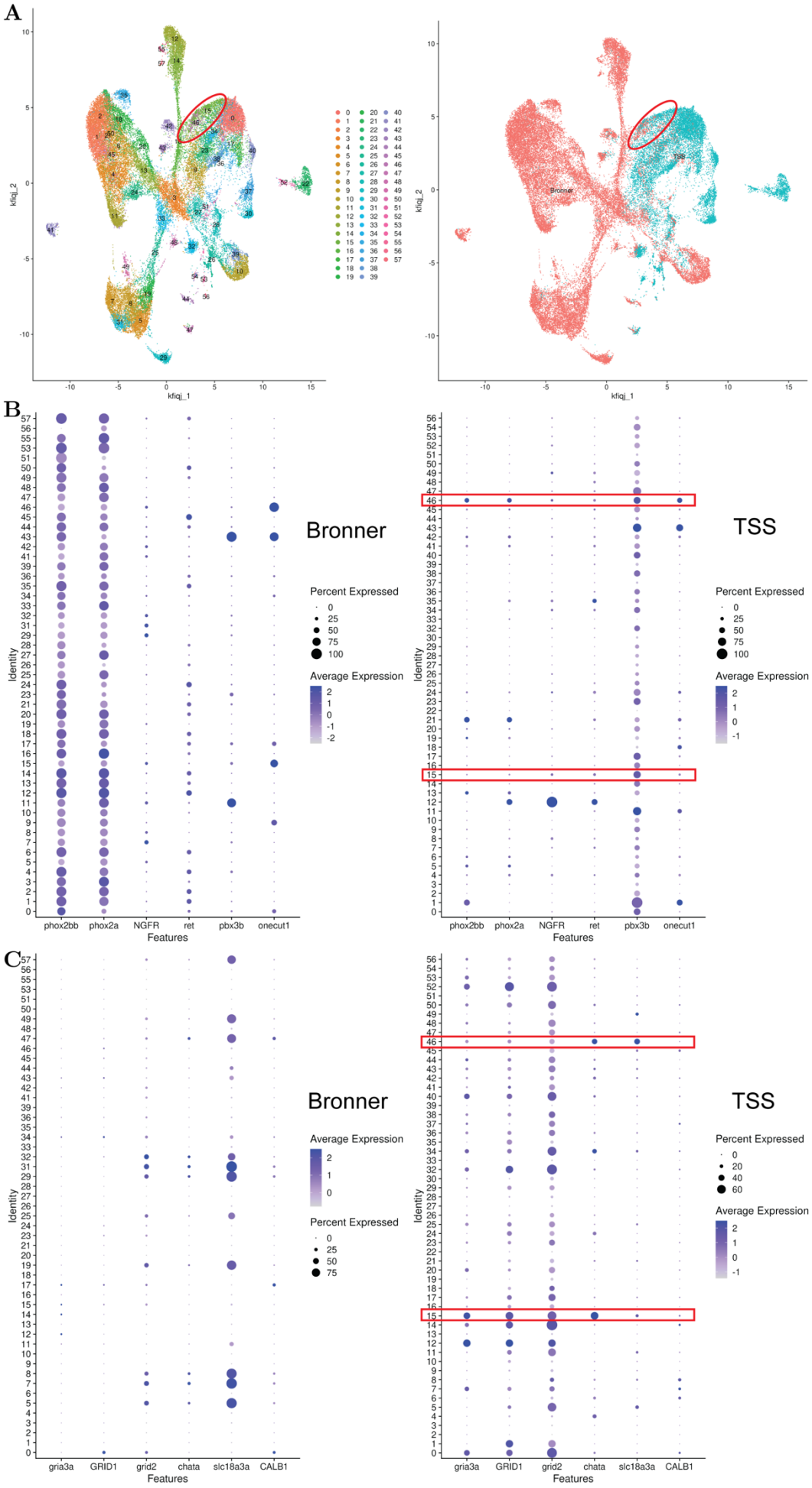
A
kfiqj_1
kfiqj_2
Bronner
TSS
B
Bronner
TSS
Identity
Features
phox2bb
phox2a
NGFR
ret
pbx3b
onecut1
Percent Expressed
Average Expression
C
Bronner
TSS
gria3a
GRID1
grid2
chata
slc18a3a
CALB1

Figure 8 – Integrative marker gene expression analysis of NMP-derived enteric neuron subtypes – (A) Integrated UMAP of neuronal subset, with the red outline showing the clusters (Clusters 46 and 15) which show significant co-clustering between TSS and Bronner datasets. (B) Dot plot showing expression of canonical markers expressed by ENS neurons in Bronner (left) and TSS (right) datasets. The red boxes outline the clusters of interest in the TSS data. (C) Dot plot showing expression of components of glutamatergic (*gria3a, grid1a, grid2*), cholinergic (*slc18a3a, chata*) and calbindin (*calb1a*) expressing neurons which are putative NMP-derived ENS neurons.

3.7 Marker gene expression analysis of other NMP-derived neuronal populations

The subset of neural cell types after filtering of expression of *elavl3/4* and *snap25a/b*, provided a dramatically increased clustering resolution, forming distinct clusters of neuron subtypes and leading to putative identification of NMP-derived enteric neuron subpopulations. Following the same strategy, we decided to use the UMAP representation of the TSS data within the integrated dataset for diving and gaining insight into some other NMP-derived neuronal populations.

Through our immunostaining data, we observed NMP contributions to the sympathetic chain ganglia which is an important component of the PNS (Figure 2). For profiling the ENS, Li et al. removed the heads and vagal NC regions of the zebrafish larvae and used the trunk region for performing scRNA-seq (Li *et al.*, 2025). Since the sympathetic ganglia have been shown to express *phox2bb (Lumb and Schwarz, 2015; Morrison et al., 2016)*, we expected the Bronner data to have captured sympathetic ganglia or their progenitors. As a result, we focused on the clusters 9 and 27 (C9, C27) which show significant co-clustering between Bronner and TSS datasets (Figure 9A). To that effect, we checked for expression of sympathetic chain ganglia marker genes. While the TSS dataset showed negligible expression of catecholaminergic enzymes like *th* and *dbh* that are markers of differentiated sympathetic ganglia, we saw notable expression of transcription factors required for specification of sympathetic ganglia, like *neurod1, neurog1, sox9b, sox10, ascl1b, insm1b,* etc (Figure 9B).

While exploring the expression of *erbb2* and *erbb3a/b*, that represent tyrosine receptor kinases involved in ErbB signalling, a process crucial for the proper differentiation of sympathetic ganglia; we stumbled upon a distinct pair of clusters which were exclusively present in the TSS data, clusters 22 and 52 (C22, C52) (Figure 9A). Astonishingly, C22 and C52 showed high expression of the ErbB signalling components, which act as survival cues for Schwann cell precursors (SCPs) associated with axons. Sympathetic chain ganglia typically arise from SCPs, which are late multipotent progenitors derived from the trunk NC but retain their multipotency to

later contribute to dorsal root ganglia (DRGs), enteric neurons, chromaffin cells of the adrenal medulla, melanocytes and sympathetic chain ganglia among other cell types (Furlan and Adameyko, 2018; Kastriti *et al.*, 2022). To further confirm their identity, we checked the expression of SCP markers known from mice studies. While C22 and C52 show a canonical glial gene expression profile of *s100b, fabp2/3, gfap,* etc., they also express SCP-specific glial marker genes which include *plp1a/b* and *mpz*. Additionally, they also express *sox10,* a transcription factor that involved in specifying SCPs. Finally, they also express vimentin (*vim*) which is a marker of a mesenchymal fate indicating that these SCPs might migrate inside the embryo (Figure 9C).

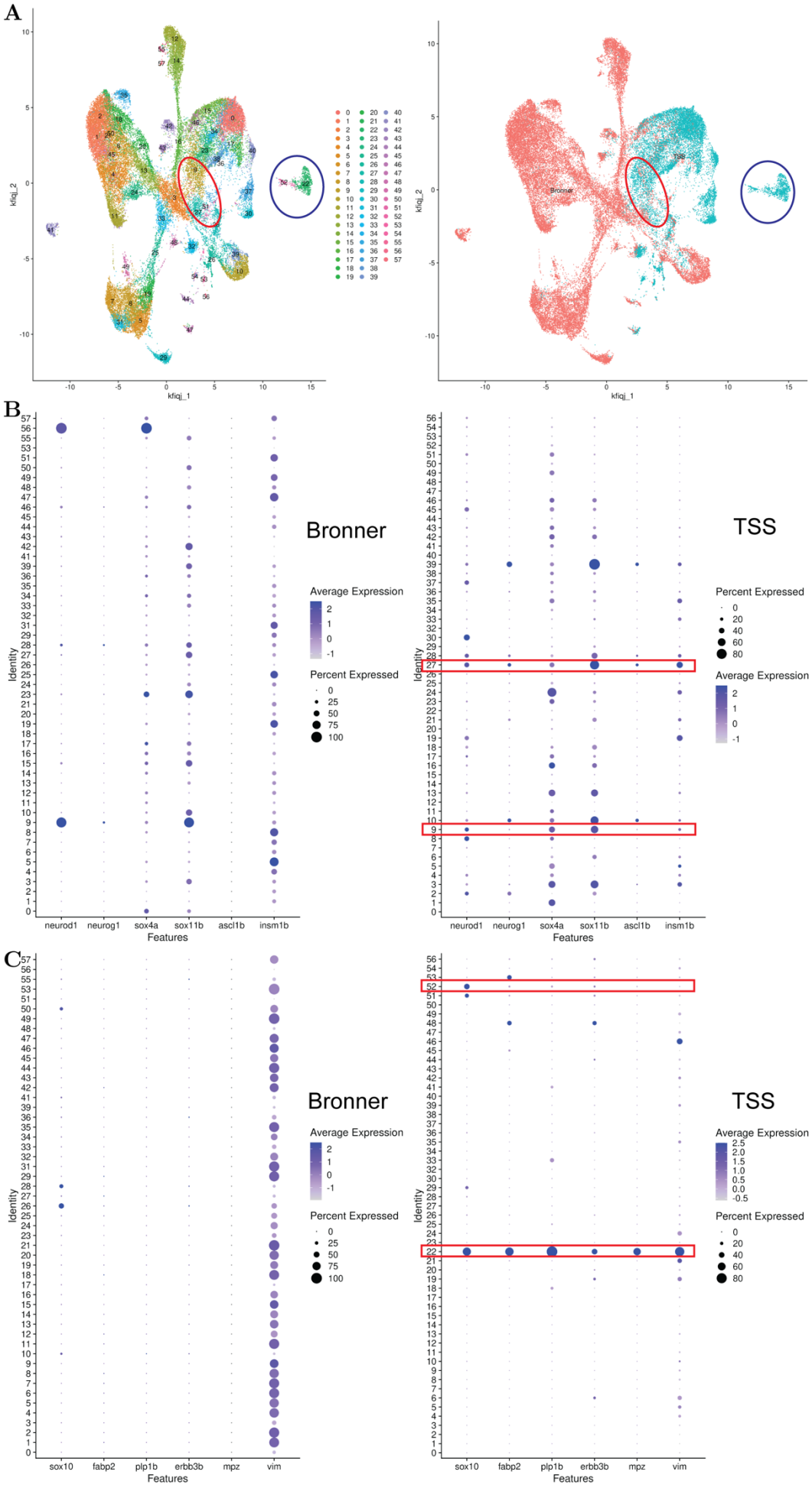
A
kfiqj_2
kfiqj_1
Bronner
TSS
B
Identity
Features
neurod1
neurog1
sox4a
sox11b
ascl1b
insm1b
Average Expression
Percent Expressed
C
sox10
fabp2
plp1b
erbb3b
mpz
vim

Figure 9 - Integrative marker gene expression analysis of NMP-derived sympathetic neuron and Schwann Cell Precursors (SCPs) subtypes – (A) Integrated UMAP of neuronal subset, with the red outline showing the clusters (Clusters 9 and 27) which show significant co-clustering between TSS and Bronner datasets. The blue outline shows the putative SCP cluster, exclusive to the TSS dataset (Clusters 22 and 52). (B) Dot plot showing expression of canonical markers expressed by symapathetic chain ganglia neurons in Bronner (left) and TSS (right) datasets. The red boxes outline the clusters of interest in the TSS data. (C) Dot plot showing expression of canonical markers of SCPs in Bronner (left) and TSS (right datasets) with the red boxes outlining the clusters of interest (Cluster 22 and 52).

Chapter 4 Discussion

In this study, we have profiled NMP derivatives in the zebrafish larva using a genetic lineage tracing system coupled with single-cell transcriptomic sequencing approach called Convert-seq. We have performed Convert-seq on zebrafish larvae spanning a wide range of developmental stages from 2 dpf till 12 dpf stages which captures crucial developmental dynamics like the formation of the enteric nervous system, differentiation of the sympathetic nervous system, and other important neuronal lineages. We also performed annotation transfer from a whole-embryo single-cell atlas called Zebrahub, and discovered the broad developmental potential of NMPs. Finally, using integrative analyses using publicly available scRNA-seq datasets, we have been able to delineate specific neuronal populations contribute to by NMPs and characterize their transcriptomic state using marker gene expression analyses.

Here, we present a genetic lineage method that is able to capture the derivatives of transient cell populations by constitutively labelling them, enabling study of complex developmental processes like cell migration, gene regulatory phenomena, and cell fate decisions at high resolution (Figure 2A). Additionally, we have also demonstrated that combining lineage tracing through cellular and nuclear labelling improves the capture of cell types which are sensitive to dissociation procedures and obtain a more unbiased and comprehensive view of the descendant cell types (Figure 5). Furthermore, using scRNA-seq and snRNA-seq, we discovered that NMPs which were traditionally thought to be a bipotent progenitor population, instead is one of the most multipotent progenitor populations in the zebrafish embryo, similar to the NC (Figure 6C).

While there have been multiple studies that have performed lineage tracing on NMPs using various methods and in diverse models, these studies have not discovered novel NMP derivatives beyond the canonical derivatives like spinal cord neurons, paraxial mesoderm and floor plate (Garriock *et al.*, 2015; Koch *et al.*, 2017; Guillot *et al.*, 2021; Lange *et al.*, 2023). While we cannot exclude the possibility of evolutionary differences in NMP derivatives within vertebrates, we speculate that these studies have been unable to capture the diversity in NMP derivatives due to the developmental stages profiled combined with the limitations of the lineage tracing method. However, a more recent study which uses high-throughput clonal lineage tracing approach has been able to capture the NC derivatives from NMPs in a mice model suggesting the possible

conservation of NMP multipotency across vertebrates (Erickson *et al.*, 2024). This raises the possibility that the true developmental potential of several progenitor populations throughout the embryo remain to be uncovered.

Using integrative analysis of the ENS scRNA-seq data from Li et al. (Li *et al.*, 2025), we discovered the NMP contributions to a population of glutamatergic neurons in the ENS. There is limited literature with regards to the zebrafish ENS development, with only three previous studies trying to characterize the cell type diversity in the ENS using single-cell transcriptomic approaches (Howard *et al.*, 2021; Kuil *et al.*, 2023; Li *et al.*, 2025). Two studies which have profiled NC-derived ENS progenitors using *phox2bb* and *sox10* expression have not described any neuronal populations expressing glutamate, which is a key excitatory neurotransmitter in the animal kingdom (Howard *et al.*, 2021; Li *et al.*, 2025). One of the studies describes a glutamatergic neuronal subpopulation which does not express *phox2bb*, however, the study does not comment upon its embryonic origin (Kuil *et al.*, 2023). However, ENS literature in mice is rich with reports of the functional importance of glutamatergic ENS neurons in regulating gut motility (Kirchgessner, 2001; Brumovsky *et al.*, 2011; Filpa *et al.*, 2016; Hamnett *et al.*, 2024). Glutamatergic neurons in the ENS are often shown to co-express acetylcholine and calbindin, which constitute the other two excitatory neurotransmitters found in the ENS (Liu *et al.*, 1997; Kirchgessner, 2001; Swaminathan *et al.*, 2019), which is in concordance with our data. Moreover, studies have also found specific glutamatergic neuronal subpopulations in the hindgut region which plays a crucial role in motor control of gut motility (Brumovsky *et al.*, 2011; Swaminathan *et al.*, 2019; Hamnett *et al.*, 2024). Based on our immunostaining data, where we observe clear NMP contributions to the posterior ENS (Figure 2C) and given that NC-derived ENS neurons do not contribute to forming enteric glutamatergic neurons (Howard *et al.*, 2021; Li *et al.*, 2025), it is tempting to speculate that these specific enteric glutamatergic neurons might be derived from NMPs.

Additionally, we focus on the expression two specific transcription factors involved in putative NMP-derived enteric neurons, *pbx3b* and *onecut1*. While *pbx3* has been shown to play a crucial role in ENS development in both mice and zebrafish (Morarach *et al.*, 2021; Li *et al.*, 2025), the role of *onecut1* transcription factor has been only described in zebrafish ENS development (Li *et al.*, 2025). The *onecut1+* gut neurons form a distinct cluster expressing neurotransmitter galanin (*gal*) and are spread in clusters throughout the gut. However, we did not observe *gal* expression in NMP-derived *onecut1+* neurons, suggesting two possibilities: First, either the NMP-derived *onecut1+* neurons are contributing to some other neuronal population and are absent from the gut. Second, NMP-derived *onecut1+* neurons are forming a functionally distinct subpopulation of neurons which express different neurotransmitter

combinations within the ENS. Based on our immunostaining data (Figure 2) and our co-clustering analysis (Figure 8), we hypothesize the second possibility to be true. However, since Schwann Cell Precursors (SCPs) are also known to contribute to parts of the ENS later during embryonic development across vertebrates (Uesaka *et al.*, 2015; Espinosa-Medina *et al.*, 2017; El-Nachef and Bronner, 2020) whether the NMP-derived posterior gut neurons are contributed through direct differentiation of NMPs or through NMP-derived SCPs (Figure 9) still remains to be investigated. The NMP-derived posterior contribution to the ENS neurons suggest that NMPs are a strong candidate for designing stem cell therapies against ENS developmental disorders like Hirschsprung disease, characterized by the hypogangliogenesis and impaired motility in the posterior gut. A recent study has also been able to successfully rescue defects in a severe mice model of Hirschsprung disease, through *in vitro* hPSC-derived NMPs (Fan *et al.*, 2023).

Another significant finding of our study is the origin of NMP-derived putative Schwann Cell Precursors (SCPs). Previous literature considered SCPs, which cover peripheral nerves throughout the body, to be a multipotent progenitor population derived from the NC (Furlan and Adameyko, 2018; Kameneva *et al.*, 2021). SCPs retain their multipotent potential and form cell type derivatives as diverse as the NC, ranging from melanocytes, chondrocytes, osteoblasts, odontoblasts, sympathetic and parasympathetic ganglia, enteric and autonomic neurons and chromaffin cells (Adameyko *et al.*, 2009; Dyachuk *et al.*, 2014; Kaukua *et al.*, 2014; Uesaka *et al.*, 2015; Furlan *et al.*, 2017; Xie *et al.*, 2019; Kastriti *et al.*, 2022). SCPs are hypothesized to have different subpopulations in the embryo, some of the known ones expressing *dhh* and *plp1b (Solovieva and Bronner, 2021).* Although we do not have any expression of *dhh* in our NMP-derived putative SCPs, we observe high *plp1b* expression (Figure 9C) in addition to several other canonical markers to detect SCPs like *mpz, erbb2, erbb3b, sox10,* etc. providing further evidence that a subset of SCPs is possibly derived from NMPs. This finding has immense implications for regenerative medicine, since SCPs are found to respond to injuries in various contexts and mount a regenerative response (Adameyko *et al.*, 2009; Johnston *et al.*, 2013; Kaukua *et al.*, 2014; Johnston *et al.*, 2016; Han *et al.*, 2017; Parfejevs *et al.*, 2018; Stierli *et al.*, 2018; El-Nachef and Bronner, 2020) and through *in vitro* studies is shown to be highly plastic (Dupin *et al.*, 2003; Real *et al.*, 2005; Kim *et al.*, 2017). Additionally, several cancers which include neurofibromas, melanomas, neuroblastomas are of glial origin and often arise from Schwann cells (Chen *et al.*, 2014; Li *et al.*, 2016), of which understanding the molecular mechanisms is crucial.

In conclusion, through this study, we provide evidence for the multipotent nature of NMPs as an embryonic progenitor population and establish NMPs as a paradigm for

studying mechanisms underlying complex cell fate decisions and lineage restriction in a multipotent progenitor system. We also discover an unprecedented range of NMP derivatives, which highlights the potential application of NMPs for studying disease-associated mechanisms and advancing regenerative cell therapies.

4. References

Achilleos, A., and Trainor, P.A. (2012). Neural crest stem cells: discovery, properties and potential for therapy. Cell Research *22*, 288-304.

Adameyko, I., Lallemend, F., Aquino, J.B., Pereira, J.A., Topilko, P., Müller, T., Fritz, N., Beljajeva, A., Mochii, M., Liste, I., Usoskin, D., Suter, U., Birchmeier, C., and Ernfors, P. (2009). Schwann Cell Precursors from Nerve Innervation Are a Cellular Origin of Melanocytes in Skin. Cell *139*, 366-379.

Bakken, T.E., Hodge, R.D., Miller, J.A., Yao, Z., Nguyen, T.N., Aevermann, B., Barkan, E., Bertagnolli, D., Casper, T., Dee, N., Garren, E., Goldy, J., Graybuck, L.T., Kroll, M., Lasken, R.S., Lathia, K., Parry, S., Rimorin, C., Scheuermann, R.H., Schork, N.J., Shehata, S.I., Tieu, M., Phillips, J.W., Bernard, A., Smith, K.A., Zeng, H., Lein, E.S., and Tasic, B. (2018). Single-nucleus and single-cell transcriptomes compared in matched cortical cell types. PLOS ONE *13*, e0209648.

Barlow, A., de Graaff, E., and Pachnis, V. (2003). Enteric Nervous System Progenitors Are Coordinately Controlled by the G Protein-Coupled Receptor EDNRB and the Receptor Tyrosine Kinase RET. Neuron *40*, 905-916.

Betancur, P., Bronner-Fraser, M., and Sauka-Spengler, T. (2010). Assembling Neural Crest Regulatory Circuits into a Gene Regulatory Network. Annual Review of Cell and Developmental Biology *26*, 581-603.

Brumovsky, P.R., Robinson, D.R., La, J.-H., Seroogy, K.B., Lundgren, K.H., Albers, K.M., Kiyatkin, M.E., Seal, R.P., Edwards, R.H., Watanabe, M., Hökfelt, T., and Gebhart, G.F. (2011). Expression of vesicular glutamate transporters type 1 and 2 in sensory and autonomic neurons innervating the mouse colorectum. Journal of Comparative Neurology *519*, 3346-3366.

Catala, M., Teillet, M.-A., and Le Douarin, N.M. (1995). Organization and development of the tail bud analyzed with the quail-chick chimaera system. Mechanisms of Development *51*, 51-65.

Chen, Z., Liu, C., Patel, Amish J., Liao, C.-P., Wang, Y., and Le, Lu Q. (2014). Cells of Origin in the Embryonic Nerve Roots for NF1-Associated Plexiform Neurofibroma. Cancer Cell *26*, 695-706.

Douarin, N.L., and Kalcheim, C. (1999). The Neural Crest. Cambridge University Press.

Dupin, E., Real, C., Glavieux-Pardanaud, C., Vaigot, P., and Le Douarin, N.M. (2003). Reversal of developmental restrictions in neural crest lineages: Transition from Schwann cells to glial-melanocytic precursors in vitro. Proceedings of the National Academy of Sciences *100*, 5229-5233.

Dyachuk, V., Furlan, A., Shahidi, M.K., Giovenco, M., Kaukua, N., Konstantinidou, C., Pachnis, V., Memic, F., Marklund, U., Müller, T., Birchmeier, C., Fried, K., Ernfors, P., and Adameyko, I. (2014). Parasympathetic neurons originate from nerve-associated peripheral glial progenitors. Science *345*, 82-87.

El-Nachef, W.N., and Bronner, M.E. (2020). De novo enteric neurogenesis in post-embryonic zebrafish from Schwann cell precursors rather than resident cell types. Development *147*.

Erickson, A.G., Isaev, S., Artemov, A., He, J., Semsch, B., Murtazina, A., Sun, J., Mangold, K., Chalou, A., Frisen, J., Ratz, M., Andersson, E., Kharchenko, P.V., and Adameyko, I. (2024). Unbiased profiling of multipotency landscapes reveals spatial modulators of clonal fate biases. bioRxiv, 2024.2011.2015.623687.

Espinosa-Medina, I., Jevans, B., Boismoreau, F., Chettouh, Z., Enomoto, H., Müller, T., Birchmeier, C., Burns, A.J., and Brunet, J.-F. (2017). Dual origin of enteric neurons in vagal Schwann cell precursors and the sympathetic neural crest. Proceedings of the National Academy of Sciences *114*, 11980-11985.

Fan, Y., Hackland, J., Baggiolini, A., Hung, L.Y., Zhao, H., Zumbo, P., Oberst, P., Minotti, A.P., Hergenreder, E., Najjar, S., Huang, Z., Cruz, N.M., Zhong, A., Sidharta, M., Zhou, T., de Stanchina, E., Betel, D., White, R.M., Gershon, M., Margolis, K.G., and Studer, L. (2023). hPSC-derived sacral neural crest enables rescue in a severe model of Hirschsprung’s disease. Cell Stem Cell *30*, 264-282.e269.

Filpa, V., Moro, E., Protasoni, M., Crema, F., Frigo, G., and Giaroni, C. (2016). Role of glutamatergic neurotransmission in the enteric nervous system and brain-gut axis in health and disease. Neuropharmacology *111*, 14-33.

Fleming, S.J., Chaffin, M.D., Arduini, A., Akkad, A.-D., Banks, E., Marioni, J.C., Philippakis, A.A., Ellinor, P.T., and Babadi, M. (2023). Unsupervised removal of

systematic background noise from droplet-based single-cell experiments using CellBender. Nature Methods *20*, 1323-1335.

Frith, T.J.R., Granata, I., Wind, M., Stout, E., Thompson, O., Neumann, K., Stavish, D., Heath, P.R., Ortmann, D., Hackland, J.O.S., Anastassiadis, K., Gouti, M., Briscoe, J., Wilson, V., Johnson, S.L., Placzek, M., Guarracino, M.R., Andrews, P.W., and Tsakiridis, A. (2018). Human axial progenitors generate trunk neural crest cells in vitro. eLife *7*, e35786.

Furlan, A., and Adameyko, I. (2018). Schwann cell precursor: a neural crest cell in disguise? Developmental Biology *444*, S25-S35.

Furlan, A., Dyachuk, V., Kastriti, M.E., Calvo-Enrique, L., Abdo, H., Hadjab, S., Chontorotzea, T., Akkuratova, N., Usoskin, D., Kamenev, D., Petersen, J., Sunadome, K., Memic, F., Marklund, U., Fried, K., Topilko, P., Lallemend, F., Kharchenko, P.V., Ernfors, P., and Adameyko, I. (2017). Multipotent peripheral glial cells generate neuroendocrine cells of the adrenal medulla. Science *357*, eaal3753.

Ganz, J. (2018). Gut feelings: Studying enteric nervous system development, function, and disease in the zebrafish model system. Developmental Dynamics *247*, 268-278.

Garriock, R.J., Chalamalasetty, R.B., Kennedy, M.W., Canizales, L.C., Lewandoski, M., and Yamaguchi, T.P. (2015). Lineage tracing of neuromesodermal progenitors reveals novel Wnt-dependent roles in trunk progenitor cell maintenance and differentiation. Development *142*, 1628-1638.

Gershon, M.D. (1999). The Enteric Nervous System: A Second Brain. Hospital Practice *34*, 31-52.

Gomez, G.A., Prasad, M.S., Wong, M., Charney, R.M., Shelar, P.B., Sandhu, N., Hackland, J.O.S., Hernandez, J.C., Leung, A.W., and García-Castro, M.I. (2019). WNT/β-catenin modulates the axial identity of embryonic stem cell-derived human neural crest. Development *146*, dev175604.

Guillot, C., Djeffal, Y., Michaut, A., Rabe, B., and Pourquié, O. (2021). Dynamics of primitive streak regression controls the fate of neuromesodermal progenitors in the chicken embryo. eLife *10*, e64819.

Hackland, J.O.S., Shelar, P.B., Sandhu, N., Prasad, M.S., Charney, R.M., Gomez, G.A., Frith, T.J.R., and García-Castro, M.I. (2019). FGF Modulates the Axial Identity

of Trunk hPSC-Derived Neural Crest but Not the Cranial-Trunk Decision. Stem Cell Reports *12*, 920-933.

Hafemeister, C., and Satija, R. (2019). Normalization and variance stabilization of single-cell RNA-seq data using regularized negative binomial regression. Genome Biology *20*, 296.

Hall, B. (2000). The neural crest as a fourth germ layer and vertebrates as quadroblastic not triploblastic. Evolution & development *2*, 3-5.

Hamnett, R., Bendrick, J.L., Robertson, K., Zhao, E.T., and Kaltschmidt, J.A. (2024). Enteric glutamatergic interneurons regulate intestinal motility. bioRxiv, 2024.2003.2024.586153.

Han, S.B., Kim, H., Lee, H., Grove, M., Smith, G.M., and Son, Y.J. (2017). Postinjury Induction of Activated ErbB2 Selectively Hyperactivates Denervated Schwann Cells and Promotes Robust Dorsal Root Axon Regeneration. J Neurosci *37*, 10955-10970.

Hao, Y., Stuart, T., Kowalski, M.H., Choudhary, S., Hoffman, P., Hartman, A., Srivastava, A., Molla, G., Madad, S., Fernandez-Granda, C., and Satija, R. (2024). Dictionary learning for integrative, multimodal and scalable single-cell analysis. Nature Biotechnology *42*, 293-304.

Heumos, L., Schaar, A.C., Lance, C., Litinetskaya, A., Drost, F., Zappia, L., Lücken, M.D., Strobl, D.C., Henao, J., Curion, F., Aliee, H., Ansari, M., Badia-i-Mompel, P., Büttner, M., Dann, E., Dimitrov, D., Dony, L., Frishberg, A., He, D., Hediyeh-zadeh, S., Hetzel, L., Ibarra, I.L., Jones, M.G., Lotfollahi, M., Martens, L.D., Müller, C.L., Nitzan, M., Ostner, J., Palla, G., Patro, R., Piran, Z., Ramírez-Suástegui, C., Saez-Rodriguez, J., Sarkar, H., Schubert, B., Sikkema, L., Srivastava, A., Tanevski, J., Virshup, I., Weiler, P., Schiller, H.B., Theis, F.J., and Single-cell Best Practices, C. (2023). Best practices for single-cell analysis across modalities. Nat Rev Genet *24*, 550-572.

Hochgreb-Hägele, T., and Bronner, M.E. (2013). A novel FoxD3 gene trap line reveals neural crest precursor movement and a role for FoxD3 in their specification. Developmental Biology *374*, 1-11.

Homma, S., Oppenheim, R.W., Yaginuma, H., and Kimura, S. (2000). Expression Pattern of GDNF, c-ret, and GFRαs Suggests Novel Roles for GDNF Ligands during Early Organogenesis in the Chick Embryo. Developmental Biology *217*, 121-137.

Howard, A.G.A.I.V., Baker, P.A., Ibarra-García-Padilla, R., Moore, J.A., Rivas, L.J., Tallman, J.J., Singleton, E.W., Westheimer, J.L., Corteguera, J.A., and Uribe, R.A. (2021). An atlas of neural crest lineages along the posterior developing zebrafish at single-cell resolution. eLife *10*, e60005.

Hu, Z., Mayes, S., Wang, W., Santos-Pereira, J.M., Theis, F., and Sauka-Spengler, T. (2024). Single-cell multi-omics, spatial transcriptomics and systematic perturbation decode circuitry of neural crest fate decisions: bioRxiv.

Johnston, Adam P.W., Naska, S., Jones, K., Jinno, H., Kaplan, David R., and Miller, Freda D. (2013). Sox2-Mediated Regulation of Adult Neural Crest Precursors and Skin Repair. Stem Cell Reports *1*, 38-45.

Johnston, Adam P.W., Yuzwa, Scott A., Carr, Matthew J., Mahmud, N., Storer, Mekayla A., Krause, Matthew P., Jones, K., Paul, S., Kaplan, David R., and Miller, Freda D. (2016). Dedifferentiated Schwann Cell Precursors Secreting Paracrine Factors Are Required for Regeneration of the Mammalian Digit Tip. Cell Stem Cell *19*, 433-448.

Kague, E., Gallagher, M., Burke, S., Parsons, M., Franz-Odendaal, T., and Fisher, S. (2012). Skeletogenic Fate of Zebrafish Cranial and Trunk Neural Crest. PLOS ONE *7*, e47394.

Kameneva, P., Kastriti, M.E., and Adameyko, I. (2021). Neuronal lineages derived from the nerve-associated Schwann cell precursors. Cellular and Molecular Life Sciences *78*, 513-529.

Kastriti, M.E., Faure, L., Von Ahsen, D., Bouderlique, T.G., Boström, J., Solovieva, T., Jackson, C., Bronner, M., Meijer, D., Hadjab, S., Lallemend, F., Erickson, A., Kaucka, M., Dyachuk, V., Perlmann, T., Lahti, L., Krivanek, J., Brunet, J.F., Fried, K., and Adameyko, I. (2022). Schwann cell precursors represent a neural crest-like state with biased multipotency. The EMBO Journal *41*, e108780.

Kaukua, N., Shahidi, M.K., Konstantinidou, C., Dyachuk, V., Kaucka, M., Furlan, A., An, Z., Wang, L., Hultman, I., Ährlund-Richter, L., Blom, H., Brismar, H., Lopes, N.A., Pachnis, V., Suter, U., Clevers, H., Thesleff, I., Sharpe, P., Ernfors, P., Fried, K., and Adameyko, I. (2014). Glial origin of mesenchymal stem cells in a tooth model system. Nature *513*, 551-554.

Kim, H.-S., Lee, J., Lee, D.Y., Kim, Y.-D., Kim, J.Y., Lim, H.J., Lim, S., and Cho, Y.S. (2017). Schwann Cell Precursors from Human Pluripotent Stem Cells as a Potential Therapeutic Target for Myelin Repair. Stem Cell Reports *8*, 1714-1726.

Kimmel, C.B., Ballard, W.W., Kimmel, S.R., Ullmann, B., and Schilling, T.F. (1995). Stages of embryonic development of the zebrafish. Developmental Dynamics *203*, 253-310.

Kirchgessner, A.L. (2001). Glutamate in the enteric nervous system. Current Opinion in Pharmacology *1*, 591-596.

Koch, F., Scholze, M., Wittler, L., Schifferl, D., Sudheer, S., Grote, P., Timmermann, B., Macura, K., and Herrmann, B.G. (2017). Antagonistic Activities of Sox2 and Brachyury Control the Fate Choice of Neuro-Mesodermal Progenitors. Developmental Cell *42*, 514-526.e517.

Korsunsky, I., Millard, N., Fan, J., Slowikowski, K., Zhang, F., Wei, K., Baglaenko, Y., Brenner, M., Loh, P.-r., and Raychaudhuri, S. (2019). Fast, sensitive and accurate integration of single-cell data with Harmony. Nature Methods *16*, 1289-1296.

Krishnakumar, R., Chen, Amy F., Pantovich, Marisol G., Danial, M., Parchem, Ronald J., Labosky, Patricia A., and Blelloch, R. (2016). FOXD3 Regulates Pluripotent Stem Cell Potential by Simultaneously Initiating and Repressing Enhancer Activity. Cell Stem Cell *18*, 104-117.

Kuil, L.E., Kakiailatu, N.J.M., Windster, J.D., Bindels, E., Zink, J.T.M., van der Zee, G., Hofstra, R.M.W., Shepherd, I.T., Melotte, V., and Alves, M.M. (2023). Unbiased characterization of the larval zebrafish enteric nervous system at a single cell transcriptomic level. iScience *26*, 107070.

Lange, M., Granados, A., VijayKumar, S., Bragantini, J., Ancheta, S., Santhosh, S., Borja, M., Kobayashi, H., McGeever, E., Solak, A.C., Yang, B., Zhao, X., Liu, Y., Detweiler, A.M., Paul, S., Mekonen, H., Lao, T., Banks, R., Kim, Y.-J., Jacobo, A., Balla, K., Awayan, K., D'Souza, S., Haase, R., Dizeux, A., Pourquie, O., Gómez-Sjöberg, R., Huber, G., Serra, M., Neff, N., Pisco, A.O., and Royer, L.A. (2023). Zebrahub – Multimodal Zebrafish Developmental Atlas Reveals the State-Transition Dynamics of Late-Vertebrate Pluripotent Axial Progenitors. bioRxiv, 2023.2003.2006.531398.

Lee, R.T.H., Knapik, E.W., Thiery, J.P., and Carney, T.J. (2013a). An exclusively mesodermal origin of fin mesenchyme demonstrates that zebrafish trunk neural crest does not generate ectomesenchyme. Development *140*, 2923-2932.

Lee, R.T.H., Thiery, J.P., and Carney, T.J. (2013b). Dermal fin rays and scales derive from mesoderm, not neural crest. Current Biology *23*, R336-R337.

Li, C., Gehring, J., and Bronner, M.E. (2025). Spatiotemporal dynamics of the developing zebrafish enteric nervous system at the whole-organ level. Developmental Cell *60*, 613-629.e616.

Li, H., Zhao, X., Yan, X., Jessen, W.J., Kim, M.O., Dombi, E., Liu, P.P., Huang, G., and Wu, J. (2016). Runx1 contributes to neurofibromatosis type 1 neurofibroma formation. Oncogene *35*, 1468-1474.

Liu, M.T., Rothstein, J.D., Gershon, M.D., and Kirchgessner, A.L. (1997). Glutamatergic enteric neurons. J Neurosci *17*, 4764-4784.

Luecken, M.D., Büttner, M., Chaichoompu, K., Danese, A., Interlandi, M., Mueller, M.F., Strobl, D.C., Zappia, L., Dugas, M., Colomé-Tatché, M., and Theis, F.J. (2022). Benchmarking atlas-level data integration in single-cell genomics. Nature Methods *19*, 41-50.

Lukoseviciute, M., Gavriouchkina, D., Williams, R.M., Hochgreb-Hagele, T., Senanayake, U., Chong-Morrison, V., Thongjuea, S., Repapi, E., Mead, A., and Sauka-Spengler, T. (2018). From Pioneer to Repressor: Bimodal foxd3 Activity Dynamically Remodels Neural Crest Regulatory Landscape In Vivo. Developmental Cell *47*, 608-628.e606.

Lukoseviciute, M., Mayes, S., and Sauka-Spengler, T. (2021). Neuromesodermal progenitor origin of trunk neural crest in vivo: bioRxiv.

Lumb, R., and Schwarz, Q. (2015). Sympathoadrenal neural crest cells: The known, unknown and forgotten? Development, Growth & Differentiation *57*, 146-157.

McGinnis, C.S., Murrow, L.M., and Gartner, Z.J. (2019). DoubletFinder: Doublet Detection in Single-Cell RNA Sequencing Data Using Artificial Nearest Neighbors. Cell Systems *8*, 329-337.e324.

Morarach, K., Mikhailova, A., Knoflach, V., Memic, F., Kumar, R., Li, W., Ernfors, P., and Marklund, U. (2021). Diversification of molecularly defined myenteric neuron classes revealed by single-cell RNA sequencing. Nature Neuroscience *24*, 34-46.

Morrison, M.A., Zimmerman, M.W., Look, A.T., and Stewart, R.A. (2016). Chapter 4 - Studying the peripheral sympathetic nervous system and neuroblastoma in zebrafish. In: Methods in Cell Biology, vol. 134, eds. H.W. Detrich, M. Westerfield, and L.I. Zon: Academic Press, 97-138.

Mosimann, C., Kaufman, C.K., Li, P., Pugach, E.K., Tamplin, O.J., and Zon, L.I. (2011). Ubiquitous transgene expression and Cre-based recombination driven by the ubiquitin promoter in zebrafish. Development *138*, 169-177.

Nagy, N., and Goldstein, A.M. (2017). Enteric nervous system development: A crest cell's journey from neural tube to colon. Seminars in Cell & Developmental Biology *66*, 94-106.

National Research Council Committee for the Update of the Guide for the, C., and Use of Laboratory, A. (2011). Guide for the Care and Use of Laboratory Animals. National Academies Press (US): Washington (DC).

Obermayr, F., Hotta, R., Enomoto, H., and Young, H.M. (2013). Development and developmental disorders of the enteric nervous system. Nature Reviews Gastroenterology & Hepatology *10*, 43-57.

Odenthal, J., and Nüsslein-Volhard, C. (1998). fork head domain genes in zebrafish. Development Genes and Evolution *208*, 245-258.

Olmsted, Z.T., and Paluh, J.L. (2021). Stem Cell Neurodevelopmental Solutions for Restorative Treatments of the Human Trunk and Spine. Frontiers in Cellular Neuroscience *15*.

Parfejevs, V., Debbache, J., Shakhova, O., Schaefer, S.M., Glausch, M., Wegner, M., Suter, U., Riekstina, U., Werner, S., and Sommer, L. (2018). Injury-activated glial cells promote wound healing of the adult skin in mice. Nature Communications *9*, 236.

Real, C., Glavieux-Pardanaud, C., Vaigot, P., Le-Douarin, N., and Dupin, E. (2005). The instability of the neural crest phenotypes: Schwann cells can differentiate into myofibroblasts. Int. J. Dev. Biol. *49*, 151-159.

Respuela, P., Nikolić, M., Tan, M., Frommolt, P., Zhao, Y., Wysocka, J., and Rada-Iglesias, A. (2016). Foxd3 Promotes Exit from Naive Pluripotency through Enhancer Decommissioning and Inhibits Germline Specification. Cell Stem Cell *18*, 118-133.

Rocha, M., Singh, N., Ahsan, K., Beiriger, A., and Prince, V.E. (2020). Neural crest development: insights from the zebrafish. Developmental Dynamics *249*, 88-111.

Sambasivan, R., and Steventon, B. (2021). Neuromesodermal Progenitors: A Basis for Robust Axial Patterning in Development and Evolution. Frontiers in Cell and Developmental Biology *8*.

Sauka-Spengler, T., and Bronner-Fraser, M. (2008). A gene regulatory network orchestrates neural crest formation. Nature Reviews Molecular Cell Biology *9*, 557-568.

Schilling, T.F., and Kimmel, C.B. (1994). Segment and cell type lineage restrictions during pharyngeal arch development in the zebrafish embryo. Development *120*, 483-494.

Schoenwolf, G.C., and Nichols, D.H. (1984). Histological and ultrastructural studies on the origin of caudal neural crest cells in mouse embryos. Journal of Comparative Neurology *222*, 496-505.

Shepherd, I., and Eisen, J. (2011). Chapter 6 - Development of the Zebrafish Enteric Nervous System. In: Methods in Cell Biology, vol. 101, eds. H.W. Detrich, M. Westerfield, and L.I. Zon: Academic Press, 143-160.

Shepherd, I.T., Beattie, C.E., and Raible, D.W. (2001). Functional Analysis of Zebrafish GDNF. Developmental Biology *231*, 420-435.

Simões-Costa, M., and Bronner, M.E. (2015). Establishing neural crest identity: a gene regulatory recipe. Development *142*, 242-257.

Simões-Costa, M.S., McKeown, S.J., Tan-Cabugao, J., Sauka-Spengler, T., and Bronner, M.E. (2012). Dynamic and Differential Regulation of Stem Cell Factor FoxD3 in the Neural Crest Is Encrypted in the Genome. PLOS Genetics *8*, e1003142.

Solovieva, T., and Bronner, M. (2021). Schwann cell precursors: Where they come from and where they go. Cells & Development *166*, 203686.

Song, Y., Miao, Z., Brazma, A., and Papatheodorou, I. (2023). Benchmarking strategies for cross-species integration of single-cell RNA sequencing data. Nature Communications *14*, 6495.

Stewart, R.A., Look, A.T., Kanki, J.P., and Henion, P.D. (2004). Development of the Peripheral Sympathetic Nervous System in Zebrafish. In: Methods in Cell Biology, vol. 76: Academic Press, 237-260.

Stierli, S., Napoli, I., White, I.J., Cattin, A.-L., Monteza Cabrejos, A., Garcia Calavia, N., Malong, L., Ribeiro, S., Nihouarn, J., Williams, R., Young, K.M., Richardson, W.D., and Lloyd, A.C. (2018). The regulation of the homeostasis and regeneration of peripheral nerve is distinct from the CNS and independent of a stem cell population. Development *145*.

Stuart, T., Butler, A., Hoffman, P., Hafemeister, C., Papalexi, E., Mauck, W.M., Hao, Y., Stoeckius, M., Smibert, P., and Satija, R. (2019). Comprehensive Integration of Single-Cell Data. Cell *177*, 1888-1902.e1821.

Swaminathan, M., Hill-Yardin, E.L., Bornstein, J.C., and Foong, J.P.P. (2019). Endogenous Glutamate Excites Myenteric Calbindin Neurons by Activating Group I Metabotropic Glutamate Receptors in the Mouse Colon. Frontiers in Neuroscience *13*.

Tran, H.T.N., Ang, K.S., Chevrier, M., Zhang, X., Lee, N.Y.S., Goh, M., and Chen, J. (2020). A benchmark of batch-effect correction methods for single-cell RNA sequencing data. Genome Biology *21*, 12.

Tzouanacou, E., Wegener, A., Wymeersch, F.J., Wilson, V., and Nicolas, J.-F. (2009). Redefining the Progression of Lineage Segregations during Mammalian Embryogenesis by Clonal Analysis. Developmental Cell *17*, 365-376.

Uesaka, T., Nagashimada, M., and Enomoto, H. (2015). Neuronal Differentiation in Schwann Cell Lineage Underlies Postnatal Neurogenesis in the Enteric Nervous System. J Neurosci *35*, 9879-9888.

Waag, R., and Bohacek, J. (2023). Single-Nucleus RNA-Sequencing in Brain Tissue. Current Protocols *3*, e919.

Wada, N., Javidan, Y., Nelson, S., Carney, T.J., Kelsh, R.N., and Schilling, T.F. (2005). Hedgehog signaling is required for cranial neural crest morphogenesis and chondrogenesis at the midline in the zebrafish skull. Development *132*, 3977-3988.

Westerfield, M. (2000). The Zebrafish Book: A Guide for the Laboratory Use of Zebrafish (Danio Rerio). University of Oregon Press.

Wolf, F.A., Angerer, P., and Theis, F.J. (2018). SCANPY: large-scale single-cell gene expression data analysis. Genome Biology *19*, 15.

Wymeersch, F.J., Wilson, V., and Tsakiridis, A. (2021). Understanding axial progenitor biology in vivo and in vitro. Development *148*.

Xie, M., Kamenev, D., Kaucka, M., Kastriti, M.E., Zhou, B., Artemov, A.V., Storer, M., Fried, K., Adameyko, I., Dyachuk, V., and Chagin, A.S. (2019). Schwann cell precursors contribute to skeletal formation during embryonic development in mice and zebrafish. Proceedings of the National Academy of Sciences *116*, 15068-15073.

Zheng, G.X.Y., Terry, J.M., Belgrader, P., Ryvkin, P., Bent, Z.W., Wilson, R., Ziraldo, S.B., Wheeler, T.D., McDermott, G.P., Zhu, J., Gregory, M.T., Shuga, J., Montesclaros, L., Underwood, J.G., Masquelier, D.A., Nishimura, S.Y., Schnall-Levin, M., Wyatt, P.W., Hindson, C.M., Bharadwaj, R., Wong, A., Ness, K.D., Beppu, L.W., Deeg, H.J., McFarland, C., Loeb, K.R., Valente, W.J., Ericson, N.G., Stevens, E.A., Radich, J.P., Mikkelsen, T.S., Hindson, B.J., and Bielas, J.H. (2017). Massively parallel digital transcriptional profiling of single cells. Nature Communications *8*, 14049.